Trace element and helium isotope geochemistry of the Cenozoic intraplate volcanism in the East Sea (Sea of Japan): Implications for lithosphere-asthenosphere interaction

Wonhee Lee[1], Hyunwoo Lee[1,*], Donghwan Kim[1], Jonguk Kim[2], Jihye Oh[1,2], Jung-Hun Song[1], Chang Hwan Kim[3], Chan Hong Park[3], Finlay M. Stuart[4]

[1]School of Earth and Environmental Sciences, Seoul National University, Seoul 08826, Republic of Korea

[2]Deep–Sea and Seabed Mineral Resources Research Center, Korea Institute of Ocean Science and Technology, Busan 49111, Republic of Korea

[3]East Sea Research Institute, Korea Institute of Ocean Science and Technology, Uljin 36315, Republic of Korea

[4]Scottish Universities Environmental Research Centre, East Kilbride G75 0QF, United Kingdom

*Corresponding author.

E-mail: lhw615@snu.ac.kr (H. Lee).

Keywords: East Asia, Dokdo, Ulleungdo, Cenozoic Intraplate volcanism, Helium isotopes, Trace elements

Abstract

Extensive intraplate volcanism in the East Asia regions, including Dokdo and Ulleungdo (DU), occurred due to the extensional stress field during the Cenozoic era. However, the origin of these magmas is still controversial. Here we report new results of helium isotopes in olivine and clinopyroxene phenocrysts as well as major and trace element compositions from the DU basalts in order to determine the origin of the DU magmas and provide insights into Cenozoic mantle dynamics in East Asia. The DU volcanic islands were formed by magmatism after opening of the East Sea (Sea of Japan), a back-arc basin behind the Japanese arc, and are currently located in the Ulleung basin, one of sub-basins of the East Sea. The $^{3}He/^{4}He$ ratios range from 5.7 to 5.9 Ra for Dokdo and 4.5 to 6.0 Ra for Ulleungdo, respectively, similar to the SCLM range of East Asia (4.6 to 7.7 Ra). Helium isotope compositions indicate that the depleted asthenosphere or the lower mantle plume might not be the direct source of the DU magmas. Also, there is no geochemical evidence that the DU magmas were influenced by subduction-derived components or the HIMU mantle source. Hence, we argue that SCLM provided enriched geochemical features in the DU basalts, contrary to basalts from other back-arc basins composed of the oceanic crust. In this respect, it is likely that the extended SCLM may still remain beneath the Ulleung basin. Our helium isotope and trace element mixing model shows the mixing trend between the metasomatized lithospheric melts and the asthenospheric melts. In addition, the presence of the low-velocity zone beneath the surface of the DU volcanoes in seismic tomography implies that the magmas were formed through the lithospheric melting due to the hot asthenospheric upwelling. Therefore, our study shows that the DU volcanism was mainly contributed by SCLM and that the lithosphere-asthenosphere interaction was the main mechanism that led to the Cenozoic magmatism in East Asia.

1. Introduction

The continental lithosphere of East Asia has undergone considerable thinning during the late Mesozoic and the Cenozoic (Liu et al., 2019 and references therein). Major extensional event started from 60 to 50 Ma due to the subduction of the Izanagi-Pacific ridge along the eastern Eurasia plate margin and the collision of the India plate (Kimura et al., 2018 and references therein). The extension proceeded as the Izanagi plate separated from the mantle transition zone and sank into the lower mantle at about 35 Ma, triggering rollback and stagnation of the Pacific plate (Liu et al., 2019 and references therein). The complex extension of the Pacific-Eurasia-India plate system created the Yinchuan-Hetao and Shanxi-Shaanxi rift systems in North China Craton, and formed marginal sea basins such as the East Sea (Sea of Japan) and South China Sea (Fig. 1a and b) (Kimura et al., 2018; Liu et al., 2019). Moreover, the extensional stress field is suggested to have caused extensive intraplate volcanism during the Cenozoic era in the North China Craton (e.g., Hannuoba, Fansi, Datong, Qixia, Kuandian, and Longgang), the Korean peninsula (e.g., Mt. Baekdu/Changbaishan, Jeongok, Boeun, Ganseong, and Baengnyeongdo; Fig. 1b), and the East Sea (e.g., Dokdo and Ulleungdo; Fig. 1b) (e.g., Choi et al., 2006; Liu et al., 2019).

The volcanism is characterized by alkaline basalts with enriched trace element patterns similar to the ocean island basalt (OIB) trend. They typically show mixing between the depleted MORB mantle (DMM) and the enriched mantle (EM) components in Sr, Nd, and Pb radiogenic isotope composition (e.g., Chen et al., 2007; Choi et al., 2006). However, controversy remains over why the magmas were enriched compared to DMM in the formation of the Cenozoic East Asian basalts. To resolve this, it has been proposed that the Cenozoic basalts were derived from the heterogeneously enriched asthenospheric mantle (e.g., Choi et al., 2006) or the East Asian asthenospheric mantle containing the stagnant Pacific slab-derived components (e.g.,

Sakuyama et al., 2013). Another scenario is that the SCLM has been melted (e.g., Wang et al., 2011) or the lithospheric mantle and the asthenospheric mantle have undergone interaction (e.g., Tang et al., 2006).

The Dokdo and Ulleungdo (DU) islands belong to the Cenozoic volcanic systems located in the East Sea back-arc basin of the Japanese arc system (Fig. 1b) and formed after the opening of the East Sea. The DU alkali basalts have similar geochemical properties to other Cenozoic basalts in East Asia, indicating a similar source of magma. For this reason, the DU volcanoes are suitable targets for investigating the magma origin of intraplate volcanism and the East Sea opening, the major plate tectonic events in East Asia in the Cenozoic era. There have been many previous studies on the DU magmas to decipher the origins of these volcanoes. Lee et al. (2002) and Nakamura et al. (1989) proposed a mantle plume origin model based on the OIB-like geochemical features in the DU magmas, but seismic tomography studies fail to provide evidence for a plume conduit beneath the region (Chen et al., 2017; Obayashi et al., 2013; Wei et al., 2012 and references therein). In addition, it has been proposed that the DU basalt geochemistry is attributed to either the involvement of the enriched asthenosphere source (e.g., Choi et al., 2006) or enriched sub-continental lithospheric mantle (SCLM) (e.g., Chen et al., 2018; Kimura et al., 2018).

In order to distinguish between these origins, we have analyzed helium isotopes in volcanic rocks from the DU islands (Fig. 1b). Helium isotopes are efficient tracers of the origin of intraplate basalts for identifying magma sources, because the inertness of helium to chemical reactions allows to preserve helium isotope compositions without being significantly affected by various geological processes. Due to the aforementioned characteristics, helium isotope ratios ($^{3}He/^{4}He$) are useful to distinguish between different mantle reservoirs. For example, depleted asthenosphere shows uniform $^{3}He/^{4}He$ ratios (8±1 Ra, where Ra is the atmospheric

$^3He/^4He$ ratio, 1 Ra = 1.39 x 10^{-6}; Graham, 2002), while fertile lower mantle has higher $^3He/^4He$ ratios than depleted mantle (> 9 Ra; Stuart et al., 2003). The $^3He/^4He$ ratios of SCLM remain poorly understood, but they are thought to have radiogenic and a wider range than the DMM, and the average $^3He/^4He$ range of the global SCLM (6.1±0.9 Ra) was reported by Gautheron and Moreira (2002). Based on the helium isotope compositions of monzonites from Ulleungdo (up to 6.4 Ra), Kim et al. (2008) suggested that the Ulleungdo felsic plutonic rocks are produced by differentiation of basaltic magmas erupted from 1.37 to 0.97 Ma (Kim et al., 1999), and that the magma was sourced in SCLM or asthenospheric melts affected of crustal assimilation. However, the helium isotope compositions of differentiated felsic rocks can be affected by degassing, diffusion, or contamination with crustal components, and mafic volcanic rocks are typically used. In this study we report new analyses of olivine and clinopyroxene phenocrysts from primitive basalts in order to (1) determine the origin of the DU magmas and (2) provide insights into Cenozoic mantle dynamics in East Asia.

2. Geological setting

Back-arc basins in the western Pacific region (Fig. 1a) have been created by extension due to subduction of the Pacific plate (e.g., Kimura et al., 2018). The East Sea (Sea of Japan) back-arc basin behind the Japanese arc, formed by the subduction of the Pacific plate beneath the Eurasian plate, is comprised of three sub-basins: Yamato, Japan, and Ulleung basins (Fig. 1b). The East Sea opening began with the crustal thinning in the early Oligocene (ca. 32 Ma) or earlier, and then the Japan and Yamato basins began to form. Seafloor spreading occurred from 28 to 18 Ma in the Japan basin and parts of Yamato basin (e.g., sites 794 and 797) (Jolivet and Tamaki, 1992; Tamaki et al., 1992). Crustal extension was most active in the early Miocene (ca. 20-15 Ma), which coincided with the opening of a pull-apart basin (Ulleung basin). Several studies (e.g., Chen et al., 2015; Shuto et al., 2015 and references therein) have suggested that

back-arc basin basalts (BABBs) from the ODP 794 and 797 sites and NE Japan had enriched characteristics due to the thick fertile SCLM beneath East Asia in the earlier opening stage (ca. 28-18 Ma). However, as the opening progressed, the contribution of SCLM gradually decreased with the continental lithosphere thinning. Instead, the effects of the asthenospheric mantle upwelling became dominant, which led to a progressive change from EM to DMM signatures of BABBs formed between about 18 and 15 Ma. After about 15 Ma, the arrival of Philippine Sea plate changed the stress field in the East Sea from transtensional to compressional, and back-arc opening gradually stopped (Jolivet and Tamaki, 1992). Unlike the Japan or Yamato basins that had formed the oceanic crust, the Ulleung basin is formed of extended continental crust (Fig. 1b) (Hirahara et al., 2015; Tamaki et al., 1992). Dokdo is a volcanic island located 210 km from the eastern coast of the Korean Peninsula, 2,000 m above the seafloor, and consists of Dongdo islet (east) and Seodo islet (west) (Fig. 1c and e). Ulleungdo island is 3,000 m above the seafloor and is located 130 km from the eastern coast of the Korean peninsula and 90 km west from Dokdo (Fig. 1d and f). The eruption ages of the DU subaerial volcanic rocks are reported to be from 2.7 to 2.1 Ma (Lee et al., 2002; Song et al., 2006) and from 1.4 Ma to 5 Ka (Kim et al., 1999), respectively, but there is no detailed information on the volcanic stratigraphy or eruption ages of the lower part of these volcanoes below sea-level. They are dominantly potassic alkali basalt to trachyte, showing similar major and trace element compositions as well as Sr, Nd, and Pb isotopes. Several studies have shown that they originated from a common source and evolved by varying degrees of fractional crystallization, and crustal assimilation and seawater alteration were minor (Kim et al., 1999; Shim et al., 2010; Song et al., 2006).

3. Samples and analytical methods

3.1. Sample information

Submarine volcanic rocks of the DU islands, Republic of Korea, were dredged by the East Sea Exploration (Onnuri R/V) conducted by the Korea Institute of Ocean Science and Technology (KIOST) in 2018 and 2019 (Fig. 1c and d). Among them, four dredged rock samples (DD-3, DD-4, UD-1, and UD-4) were selected for this study (Fig. S1d, e, g, and h). DD-3 and DD-4 were from the northwestern slope of Dokdo at a depth of 573 m (Fig. 1c). UD-1 was from the northeastern slope of Ulleungdo at a depth of 1,354 m, and UD-4 was from the southern slope of Ulleungdo at a depth of 2,114 m (Fig. 1d). In addition, three subaerial basaltic agglomerate samples (DD-2, UD-2, and UD-3) were collected from the 2018 DU field campaign (Fig. S1b, c, and f). DD-2 was sampled from the edge of Dongdo that is the east islet of Dokdo, while UD-2 and UD-3 were sampled from the southern coastline of Ulleungdo (Fig. 1c and d). Core sample DD-1 was acquired by a drilling project carried out by KIOST in 2011 (Fig. S1a). DD-1 was obtained from the southern submarine site located between Dongdo and Seodo (west islet of Dokdo) (Fig. 1c).

All of the basaltic rock samples from DU exhibit porphyritic and intergranular texture, and show a variety of characteristics ranging from vesicular to dense. The phenocryst modes and other petrographic descriptions are summarized in Table 1. UD-1 has euhedral to subhedral phenocrysts of olivine, plagioclase, and small amounts of clinopyroxenes and opaque minerals, and the groundmass is composed of acicular plagioclases, olivines, and opaque minerals. Some plagioclase phenocrysts have a sieve texture (Fig. S2c). Also, most of the plagioclase phenocrysts show various degrees of patch zoning. All Dokdo samples (DD-1, DD-2, DD-3, and DD-4) are less vesicular and contain euhedral to subhedral phenocrysts of olivine, clinopyroxene, plagioclase, and opaque minerals such as magnetite or ilmenite, and the groundmass is composed of the acicular plagioclases, clinopyroxenes, opaque minerals, and minor olivines (Fig. S2a, e, and f). DD-1 and DD-2 contain olivines that have been almost altered to iddingsite, and clinopyroxenes of considerable size (up to 7 mm in diameter). Most

clinopyroxenes and plagioclases appear to have various degrees of zoning, and some olivines show also weakly normal or reverse zoning. Some samples display a poikilitic texture that subhedral clinopyroxenes include small euhedral olivine grains (Fig. S2f). Most of the Ulleungdo samples (UD-2, UD-3, and UD-4) contain some vesicles with varying size and irregular shape, and have euhedral to subhedral phenocrysts of clinopyroxene, plagioclase, and opaque minerals such as magnetite or ilmenite, and the groundmass is composed of the acicular plagioclases, clinopyroxenes, and opaque minerals (Fig. S2b, d, g, and h). UD-4 especially shows the more glassy and vesicular matrix than other samples (Table 1, Fig. S2b). The Ulleungdo subaerial samples (UD-2 and UD-3) have a considerable size of clinopyroxene and plagioclase glomerocrysts up to 5 mm (Fig. S2g and h). There are clinopyroxenes and plagioclases with the variable patchy or oscillatory zoning, as well as the ophitic clinopyroxenes in these samples (Fig. S2d). All samples show various degrees of alteration, especially near cracks or vesicles.

3.2. Analytical methods

3.2.1. Major and trace element analyses for whole-rock compositions

Whole-rock samples were milled to powder and major (Si, Al, Fe, Mg, Ca, Na, K, and Ti) and minor element (Mn and P) compositions determined by X-Ray fluorescence spectrometer (SHIMADZU XRF-1800) at the Cooperative Laboratory Center, Pukyong National University, Republic of Korea (Kim et al., 2009). Trace elements were analyzed by the NWR 193 laser ablation system coupled to Agilent 7000x Inductively Coupled Plasma Mass Spectrometer (LA-ICP-MS) at the KIOST, Republic of Korea. The analyses were carried out with a circular spot size of 105 μm, a repetition rate of 5 Hz, and pulse energy of 5 J/cm^2. Each analysis consisted of 40 seconds of measurement against background and 40 seconds of ablation. The external standard was NIST 612 glass, with ^{43}Ca for the internal standard which was previously

measured by XRF. The standard reference material for the unknown standard was BCR-2G glass, and precision (% RSD) was < 3% for most elements, < 5% for Sm, Ho, Yb, Ta, and Pb, and < 8% for Cr.

3.2.2. Major and trace element analyses for phenocryst compositions

Back-scattered electron (BSE) images and measuring major (Si, Al, Fe, Mg, Ca, and Na) and minor elements (Cr, Mn, and K) of olivine, clinopyroxene, and plagioclase were performed using a JEOL JXA-8530F field emission electron probe microanalyzer (FE-EPMA) at the National Center for Inter-University Research Facilities (NCIRF), Seoul National University, Republic of Korea. An accelerating voltage of 15 kV, a beam current of 20 nA, and a beam size of 3 μm were used. The standard minerals used for analysis were olivine, augite, and plagioclase from Smithsonian Institution (NMNH 111312-44, 164905, and 115900, respectively). Relative standard deviations of precision (% RSD) were mostly < 1% for major elements, except for FeO in olivine and clinopyroxene (< 1.5% and < 3.1%, respectively), and for Na_2O in plagioclase (< 1.2%). Trace elements for phenocrysts were analyzed in-situ by LA-ICP-MS at KIOST. The analyses were performed under conditions of a circular spot sized 105 μm for the mounts and 90 μm for thin sections, a repetition rate of 5 Hz, and pulse energy of 3 J/cm^2. Each analysis consisted of the same conditions with the whole rock analyses. The external standard was NIST 612 glass, with ^{43}Ca for the internal standard of clinopyroxene and plagioclase and ^{29}Si for olivine, which was previously measured by EPMA. The BCR-2G glass was used as the reference material for the unknown standard, and precision (% RSD) was < 3% for most elements, < 5% for Li, Ba, Sm, Eu, Dy, Tm, Yb, Lu, Hf, Ta, and Pb and <10% for Cr and Ni. It is thought that ^{45}Sc was influenced by interference with $^{29}Si^{16}O$.

3.2.3. Helium isotope analysis

Helium isotopes were measured in ~1 g of 0.25–2 mm of alteration-free olivine and

clinopyroxene phenocrysts. Grains were picked from crushed rock, washed with distilled water and ethanol using an ultrasonic cleaner. Gases in fluid inclusions were extracted by vacuum crushing phenocrysts in a multi-sample hydraulic crusher. The extracted gases were purified by exposure to two hot GP50 Zr-Al alloy getters and the heavy noble gases (Ar, Kr, and Xe) were absorbed onto a charcoal trap at the liquid nitrogen temperature before each analysis. $^{3}He/^{4}He$ ratios were measured on a ThermoFisher Helix-SFT mass spectrometer in static mode at Scottish Universities Environmental Research Centre (SUERC), United Kingdom (Stuart et al., 2000). Blank levels were measured prior to each ample exceeded 1% of the measured He. Mass spectrometer sensitivity and mass fractionation were determined by repeated analysis of aliquots from a reservoir of the Helium Standard of Japan (HESJ) international standard (20.63 Ra; Matsuda et al., 2002). The reproducibility of He isotope ratios is typically 1% (1r).

4. **Results**

4.1. Whole-rock compositions

All samples (Table 2) are displayed in the alkaline fields and are classified into four types by total alkali versus silica (TAS) diagram (Fig. 2; Le Bas et al., 1986): tephrite (DD-4), alkali basalt (DD-2), trachy-basalt (DD-1, DD-3, UD-1, UD-2, and UD-4), and basaltic trachy-andesite (UD-3). They have relatively low SiO_2 (44.9–51.3 wt.%) with Mg# [100*Mg/(Mg+Fe^{2+}) assuming Fe^{2+}/Fe^{tot}=0.9] ranging from 29.2 to 58.3. The samples are shown within the range of the other previously reported DU volcanic rock data and are categorized into relatively mafic rocks (e.g., alkali basalt to basaltic trachy-andesite) despite their lower MgO contents than high-MgO samples of DU (Figs. 2 and 3). Our CIPW normative calculations show that they are all olivine-normative (7.7–13.7%) but have no quartz (Table 2). 6 samples have normative nepheline (3.5–7.5%) except for the UD-2 and UD-3 which have hypersthene (0.8–2.6%) instead. There are negative correlations between MgO and SiO_2, Al_2O_3,

Na_2O, and K_2O, while positive correlations are shown between MgO and Fe_2O_3, CaO, CaO/Al_2O_3, and TiO_2 (Fig. 3a–h).

The chondrite-normalized rare earth element (REE) patterns are shown in Fig. 4a. All samples have enriched REE concentrations (ΣREE=231.6–325.1 ppm) than chondrite (ΣREE=2.56 ppm; Sun and McDonough, 1989). REE patterns show enrichment of light rare earth elements (LREE) with high $(La/Yb)_N$ ratios of 17.3–29.0 but relatively fractionated heavy rare earth elements (HREE) with high $(Dy/Yb)_N$ ratios of 1.5–1.9, which is similar to the typical OIB pattern, as well as NCC Cenozoic basalts (e.g., Qian et al., 2015). Only UD-1 shows a positive Eu anomaly (Fig. 4a).

Primitive mantle-normalized trace element patterns are given in Fig. 4b. All patterns show enrichment of large ion lithophile elements (LILE) and no depletion of high field strength elements (HFSE; e.g., Nb and Ta), which is also similar to the typical OIB and NCC Cenozoic basalt patterns. Most of Ulleungdo samples also have the positive anomaly of Ba. UD-1 shows positive anomalies of Ba, Sr, and Eu, attributed to plagioclase accumulation. The Pb positive anomaly is observed in most samples.

4.2. Mineral chemistry of phenocrysts

Olivine phenocrysts are common in the Dokdo basalt samples but appear to be less common in the Ulleungdo basalts (except for UD-1). Fo contents in the Dokdo samples range from 76 to 84 and 80 to 83 in the Ulleungdo basalts (Table S1), which are lower than the mantle peridotite range found in the Korean peninsula (89.2–91.0; Choi et al., 2005). NiO and CaO (0.06–0.19 and 0.19–0.38 wt.%) contents in the olivines show positive correlations with Fo contents (Fig. S3a and b), implying that the magmas have undergone fractional crystallization. Both U and Th concentrations of all olivines are below the detection limit.

Clinopyroxene phenocrysts are observed in all DU samples. Clinopyroxenes in the Dokdo samples show slightly higher Mg# values ranging from 76 to 88 ($Wo_{45.3-49.7}En_{37.9-48.1}Fs_{6.6-12.6}$) than that of the same minerals in the Ulleungdo samples with the range of 72 to 82 ($Wo_{45.3-49.8}En_{36.2-48.3}Fs_{6.4-14.6}$), except for a high Mg# value of 88.4 from one phenocryst in UD-4 (Table S2). All clinopyroxenes are classified into diopside (Fig. S4a), and Na_2O, TiO_2, Cr_2O_3, and CaO correlate with Mg# (Fig. S3c–f). This feature is different from mantle peridotites in the Korean peninsula (Fig. S3c–f). U contents of clinopyroxenes are up to 0.07 ppm and 0.03 ppm in the DU samples, respectively. Ranges of Th concentrations of clinopyroxenes are 0.02 to 0.47 ppm and 0.04 to 0.28 ppm in the DU samples, respectively.

Plagioclase phenocrysts in the DU samples are made up of labradorite to bytownite (Table S3 and Fig. S4b; $An_{62-86}Ab_{13-33}Or_{1-5}$ in Dokdo and $An_{54-87}Ab_{12-40}Or_{1-7}$ in Ulleungdo). Fe-Ti oxides analyzed in DD-3 and UD-3 can be divided into two groups: the titanomagnetite group with a relatively low TiO_2 concentration ranging from 17.3 to 18.4 wt.%. and the ilmenite group with a high TiO_2 concentration ranging from 47.8 to 48.9 wt.% (Table S4).

4.3. Helium isotope compositions

Helium concentrations and isotope compositions of the DU samples are given in Table 3. Total ^4He concentrations range from 1.3 to 2.5 x 10^{-8} ccSTP/g for olivines and from 2.8 to 96.6 x 10^{-9} ccSTP/g for clinopyroxenes. $^3He/^4He$ ratios range from 4.7 to 5.9 Ra for olivines and from 4.5 to 6.0 Ra for clinopyroxenes. $^3He/^4He$ ratios between the Dokdo (5.7–5.9 Ra) and Ulleungdo (4.5–6.0 Ra) samples do not show a significant difference. Moreover, there is no correlation between total ^4He concentrations and $^3He/^4He$ ratios (Fig. 5). The range of $^3He/^4He$ ratios from the DU basalts overlaps with the value of SCLM from East Asia (4.6-7.7 Ra; Chen et al., 2007; Kim et al., 2005) and is lower than $^3He/^4He$ ratios of mid-ocean ridge basalt (MORB; 8±1 Ra) or OIB related to hot mantle plumes (> 9 Ra).

Our single-step crushing extraction procedure does not remove lattice-hosted radiogenic or cosmogenic He (Carracedo et al., 2019). It is possible that radiogenic ^{4}He produced within crystal lattice may recoil or diffuse into fluid inclusion (e.g., Stuart et al., 2000). The proportion of radiogenic ^{4}He that is released by crushing likely depends on the proportion of voids within the minerals. The absence of a relationship between ^{4}He content and helium isotopic composition (Fig. 5) likely means that there has been no significant release of radiogenic helium.

Olivine and clinopyroxene phenocrysts in the DU rocks show relatively uniform $^{3}He/^{4}He$ ratios of 4.5 to 6.0 Ra. While whole-rock compositions are thought to represent evolved magma, the olivine and clinopyroxene phenocrysts are more primitive or in equilibrium with whole-rock melt compositions (Fig. 6). The Mg# of the melt in equilibrium with olivine and clinopyroxene phenocrysts can be calculated as follows:

$$K_D(Fe-Mg)^{min-melt} = \frac{X_{Fe}{}^{min} X_{Mg}{}^{melt}}{X_{Mg}{}^{min} X_{Fe}{}^{melt}} \quad (1)$$

$$Mg\#^{melt} = \frac{100}{(100/Mg\#^{min}-1)/K_D(min/liq)+1} \quad (2)$$

where the abbreviation 'min' in the equations means mineral such as olivine and clinopyroxene, and K_D(min/liq) is the Fe-Mg exchange coefficient between mineral and melt, known as 0.30 ± 0.03 for olivine and 0.275 ± 0.067 for clinopyroxene, respectively (Putirka et al. 2008). In the case of DD-3, some olivine phenocrysts are less primitive than the melt composition, but are in equilibrium with relatively primitive melts of Mg# ranging from 55.2 to 63.3 with K_D(ol/liq)=0.33 (Fig. 6a). In particular, UD-3 has a low whole-rock Mg# of 29.2, indicating that the melt composition is considered highly evolved, but shows similar Mg# of clinopyroxenes to other less evolved samples (Fig. 6b). Additionally, assuming the highest K_D for both olivine and clinopyroxene, all olivines and clinopyroxenes are in equilibrium with

melts in the Mg# ranges of 51.1 to 63.4 and 45.6 to 71.5, respectively, reaching the Mg# range of primary magma (68–75; Frey et al., 1978). Thus, $^{3}He/^{4}He$ ratios of olivine and clinopyroxene phenocrysts from the DU basalts might represent the relatively primitive volatile compositions of the magmas.

5. Discussion

5.1. Diagnosis of seawater alteration

The majority of samples (DD-2, DD-3, DD-4, UD-1, and UD-4) have low LOI values (0.04–2.53 wt.%). The high values of samples DD-1, UD-2, and UD-3 indicate that they have suffered alteration. It is likely that most samples were altered by seawater because they were collected from coastal and submarine environments by dredging or drilling. Thus, fluid-mobile elements (e.g., Ba, Rb, and K) might have been affected by shallow-level alteration. However, fluid-immobile elements, such as REE, HFSE (e.g., Nb, Ta, Zr, Hf, and Ti), Y, Th, and U are likely unaffected. Considering that DU samples show good correlations between Nb (or Zr) and Rb, Pb, REE, Hf, Ta, Th, and U, the effect of alteration to trace elements is insignificant (Fig. S5). Therefore, we mainly used the immobile elements in order to argue the following discussion. Moreover, our samples might not be significantly affected by seawater alteration on the basis of the chemical alteration index using the relationship between alkaline components (Na_2O+K_2O, wt%) and Na_2O/K_2O ratios (Fig. S6). Therefore, seawater alteration in our samples is thought to be minor.

5.2. Magma sources of the DU basalts

5.2.1. Crustal contamination

Crustal contamination can be examined by using the Nb/U and Ce/Pb ratios, which are less likely to be modified by fractional crystallization of silicate minerals or partial melting due to

similar compatibilities of those elements. Nb/U ratios of the DU basalts range from 37.2 to 73.4, and Ce/Pb ratios are from 17.0 to 29.0. In Fig. 8, the elemental ratios are not similar to the continental crust values which are similar to arc magmas (Rudnick and Gao, 2003), but they are closer to the MORB and OIB ranges (Hofmann et al., 1986). Although Nb/U ratios seem to follow the simple mixing line between DD-3 and the continental crust (Rudnick and Gao, 2003), at least the Ce/Pb ratio cannot be explained by crustal assimilation. Additionally, trace element patterns are different from the bulk continental crust composition, except for slightly positive anomalies of Pb (Fig. 4b). Therefore, the effect of crustal contamination was insignificant in the DU samples.

5.2.2. Fractional crystallization effect

The DU samples have a Mg# range of 29.2 to 58.3, which is lower than the primary magma (68-75; Frey et al., 1978). Thus, they may have been affected by fractional crystallization in the magma chamber or during magma ascent. Since olivine, clinopyroxene, plagioclase, and Fe-Ti oxides are the major phenocrysts, fractional crystallization of the minerals can be investigated with Harker diagrams and trace element patterns (Fig. 3 and 4). SiO_2 has a negative correlation and Ni has a positive correlation, with MgO (Fig. 3a and i), indicating fractionation of olivine. In addition, a positive correlation of CaO/Al_2O_3 and negative correlations of SiO_2 and Al_2O_3 for MgO (Fig. 3a, c, and d) reflect clinopyroxene accumulation/loss, rather than plagioclase. In most REE patterns (Fig. 4a), no negative anomaly in Eu is observed, which also indicates limited crystallization of plagioclase. In the case of UD-1, positive anomalies of Ba, Sr, and Eu (Fig. 4b) are thought to reflect that accumulation of plagioclase and do not represent the actual melt composition. Fe-Ti oxides are abundant in the DU volcanic rocks, particularly in the subaerial samples (UD-2 and UD-3), which is associated with the pattern of decreasing Fe_2O_3 and TiO_2 together when MgO decreases (Fig. 3e and f). Although crystallization of Fe-

Ti oxides can reduce Nb and Ta concentrations due to D_{Nb} and D_{Ta} with values of >1 in Ti-bearing oxides (Klemme et al., 2006 and references therein), DU volcanic rocks show that Nb and Ta increase as MgO decreases (Fig. 3j and k). This implies that the measured Nb and Ta concentrations are insignificantly affected by Fe-Ti oxide crystallization.

The basaltic rocks of DU were affected by fractional crystallization, which caused changes in major and trace element concentrations to a certain extent. However, ratios (e.g., Zr/Y, Nb/Ta, La/Yb, Nb/La, and Nb/U) between most incompatible elements (e.g., REE and HFSE) which are not partitioned into mainly crystallizing phases (e.g., olivine, clinopyroxene, and plagioclase) on basaltic magmas, are not to be changed by moderate fractional crystallization. In our data, they are also not clearly correlated with MgO (Fig. 3l–n), indicating that the incompatible trace element ratios were not critically changed by fractional crystallization.

5.2.3. Effect of magma evolution on helium isotopes

Kim et al. (2008) measured helium isotope compositions of hornblende, biotite, and feldspar in monzonite on Ulleungdo. Biotites and feldspars of Ulleungdo monzonite are known to undergo helium diffusion-controlled isotope fractionation, rather than degassing effect which causes higher $^{4}He/^{40}Ar^{*}$ values of the samples (Kim et al., 2008). Biotites and feldspars are well-matched with the diffusive fractionation model (Harrison et al., 2004), which indicates the biotites and feldspars are much affected by diffusion than hornblendes, resulting in lower $^{3}He/^{4}He$ ratios than the actual source value (Kim et al., 2008). This might be owing to lower closure temperatures of biotites and feldspars than hornblendes (Baxter, 2010 and references therein). Our $^{3}He/^{4}He$ ratios from olivines and clinopyroxenes in the DU basaltic rocks show similar values to that of hornblende from the Ulleungdo monzonite (Fig. 7; Kim et al., 2008). Because olivines and clinopyroxenes have similar to higher closure temperatures than hornblende (Baxter, 2010 and reference therein), our olivines and clinopyroxenes data might

also preserve relatively primitive $^{3}He/^{4}He$ values. The basaltic rocks from DU are considered to have similar ages to the stage-1 basaltic agglomerates about 2.47 to 2.06 Ma for Dokdo and 1.37 to 0.97 Ma for Ulleungdo, respectively (Kim et al., 1999; Lee et al., 2002). Whereas, ages of monzonite from Ulleungdo is about 0.29 to 0.12 Ma (Kim et al., 2008), younger than basalt samples. Considering the age range of the volcanic rocks of DU (2.47 to 0.12 Ma), the uniform $^{3}He/^{4}He$ ratios of minerals, such as olivine, clinopyroxene, and hornblende (Fig. 7) support that the volatile compositions in the magmas did not change significantly from the formation of the DU volcanoes to the late evolutionary stage. In other words, assuming that Ulleungdo monzonite evolved from basaltic magma by fractional crystallization (e.g., Chen et al., 2018; Kim et al., 2008; Lee et al., 2002; Song et al., 1999), we suggest that the initial helium isotope compositions were well preserved during magma evolution, as it does not appear to be significantly affected by late-stage crustal contamination or degassing. Thus, the measured $^{3}He/^{4}He$ ratios can represent the magma origin (Kim et al., 2008).

5.2.4. Mantle geochemistry

The $^{3}He/^{4}He$ ratios of the DU basalts (4.5-6.0 Ra) and Ulleungdo monzonites (5.9-6.4 Ra; Kim et al., 2008) are more radiogenic than MORB (Fig. 5). It is unlikely that they originated directly from DMM, and the lower mantle component does not seem to be the main component of the magmas due to the low $^{3}He/^{4}He$ ratios. The $^{3}He/^{4}He$ ratios are indicative of recycled components which may have low He contents and can be overprinted as the melts/fluids rise through the He-rich asthenospheric mantle (Day et al., 2015; Staudacher and Allègre, 1988). The DU $^{3}He/^{4}He$ ratios are similar to the values from other tectonic environments (Fig. 9): island/continental arc regions (2.2–7.3 Ra; Hilton et al., 2002), HIMU (4.3–9.5 Ra; Graham et al., 1992; Hanyu and Kaneoka, 1997), and continental basalts (4.5–8.6 Ra from Kenya rifts of East African Rift, Western Antarctic Rift, and eastern North China Craton; Chen et al., 2007;

Halldórsson et al., 2014; Nardini et al., 2009; Xu et al., 2014). Therefore, we would like to discuss each of these candidates showing helium isotope compositions similar to the DU rocks.

It is known that there is a stagnant Pacific slab in the mantle transition zone beneath East Asia including the East Sea (e.g., Chen et al., 2017; Wei et al., 2012). Previous studies have proposed that the East Asian Cenozoic magmatism was affected by recycled materials derived from the stagnant slab (e.g., Sakuyama et al., 2013, 2014). However, the depletion of HFSE (e.g., Nb and Ta), typical in magmas of subduction zones, is not observed in our samples (Fig. 4b). This is distinctive from the NE Japan arc basalts derived from the subduction of the Pacific plate (Fig. 4; Yamamoto and Hoang, 2009). Similarly, the Cenozoic basalts in NE China with significantly comparable geochemical characteristics to DU do not also show the depletions of HFSEs (Fig. 4b). The youngest basalts at NE China, such as Longgang, Jingbohu, and Wudalianchi, actually show significant ^{230}Th excesses in U-series disequilibria, which strongly argues against slab involvement as well (e.g., Zou et al., 2008). Moreover, geochemical studies on the ODP 794 and 797 sites of the East Sea have suggested the existence of the depleted asthenospheric mantle beneath the East Sea from about 18 Ma (e.g., Chen et al., 2015; Shuto et al., 2015), which is contrary to the model that the asthenosphere underneath the East Sea was enriched by subduction or plume-derived materials to be the source of the DU Cenozoic magmatism (Choi et al., 2006). As a result, the effect of slab-derived fluids or melts might be insignificant to make the asthenosphere beneath the East Sea hydrated and enriched (e.g., Hirahara et al., 2015; Shuto et al. 2015; Tamaki et al., 1992). In other words, the presence of a stagnant Pacific slab in the mantle transition zone does not necessarily indicate material contributions to magma generations. For the above reasons, it is inferred that the helium isotope composition of the asthenosphere underneath the East Sea is similar to the typical MORB value (8 ± 1 Ra), and the DU magmas might not be derived directly from the depleted asthenospheric mantle over the stagnant slab. Furthermore, we use ΔNb value [ΔNb = 1.74 + log (Nb/Y) - 1.92

log (Zr/Y)], which is a useful indicator for identifying source depletion by degrees of partial melting or melt extraction (Fitton et al., 1997). ΔNb > 0 implies the enriched mantle source (e.g., plume), and ΔNb < 0 value means depleted upper mantle source (Fitton et al., 1997). All DU rock samples have values of ΔNb > 0 (0.078–0.30), which supports that the magmas did not originate from the depleted asthenospheric mantle source.

The helium isotope compositions of the DU samples are similar to those of the HIMU mantle component (4.3–9.5 Ra; Graham et al., 1992; Hanyu and Kaneoka, 1997). The trace element and radiogenic isotope compositions of the DU basaltic rocks are not consistent with a significant HIMU contribution, but instead have been reported to be shown in the mixing trend between DMM and EM1 (Fig. S7) (e.g., Chen et al., 2018; Choi et al., 2006). Therefore, the HIMU source would not account for the lower helium isotope ratios than MORB for the DU magmas. Excluding the aforementioned subducting slab or HIMU components, we argue that SCLM may contribute to the formation of the DU magmas. The range of helium isotope compositions in the DU rocks overlaps with the values of SCLM and the global Cenozoic continental basalts (e.g., basalts from NKR, SKR, WAR, and NE China) (Fig. 9). The DU basalts exhibit higher concentrations of incompatible elements without depletion of Nb, Ta, and Ti, thus exhibiting the hump-shaped OIB-like trend like other continental basalts (e.g., NCC Cenozoic basalts) rather than arcs (Fig. 4).

It has been suggested that the Ulleung basin is composed of extended continental crust despite the thinning of the plate due to the back-arc opening (e.g., Tamaki et al., 1992). This allows for the possibility of the SCLM underneath DU. A few studies have reported helium isotope compositions in the mantle xenoliths found in Korea (e.g., Mt. Baekdu, Baegnyongdo, Jeju, and Jogokni) and NE China (e.g., Long Quan, Jingbohu, Kuandian, and Longgang) using the crushing method, with the ranges of 4.6 to 7.7 Ra and 4.8 to 7.2 Ra, respectively (Chen et

al., 2007; Kim et al., 2005). Helium isotope ratios of olivine and clinopyroxene from the DU basalts (4.5–6.0 Ra) and hornblende from the Ulleungdo monzonite (5.9–6.4 Ra; Kim et al., 2008) are included in the range of the xenoliths (Fig. 7 and 9), implying that helium of the DU volcanic rocks can be derived from the SCLM.

The SCLM beneath East Asia including the East Sea, the Korean peninsula, and eastern China has been suggested to provide a more enriched magma source than DMM for the Cenozoic volcanism in the region (e.g., Kim et al., 2005, 2008; Wang et al., 2011). There is evidence that the East Asian mantle xenoliths are heterogeneously metasomatized resulting in the fertile lithospheric mantle composition (Choi et al., 2006; Kim et al., 2005; Liu et al., 2019 and references therein). It has been suggested that the ancient and cold refractory SCLM beneath eastern Asia was replaced by the hot and fertile juvenile SCLM through metasomatism related to the subduction of the Paleo-Pacific plate during the Middle Jurassic to the Early Cretaceous (Liu et al., 2019 and references therein). The East Asian SCLM has shown variously fertile geochemical characteristics, such as enriched incompatible element (e.g., LREE) patterns due to various metasomatic degrees and agents (e.g., eclogitic melts from delaminated lower crust, carbonated melts/fluids from subducted crustal materials, and aqueous fluids from introduced slab components; Choi et al., 2006; Kim et al., 2005; Liu et al., 2019). Moreover, the presence of the enriched lithospheric mantle beneath the East Sea has been raised based on geochemical features of BABBs formed in the early opening stage (ca. 28-18 Ma), as discussed in section 2 (e.g., Chen et al., 2015; Shuto et al., 2015). Thus, the enriched geochemical properties of the DU volcanic rocks may imply that the SCLM contribution was significant.

5.3. Implications for lithosphere-asthenosphere interaction

Since the DU basalts are found in the East Sea, the back-arc basin, we compare the basalts of other back-arc basin settings which are known to be produced by the upwelling of

the asthenospheric mantle. Back-arc basins are formed behind the arc front due to lithosphere thinning of the overlying plate by rollback or frictional drag of the subducting slab (e.g., Elsasser, 1971; Uyeda and Kanamori, 1979). BABBs, which exhibit similar geochemical characteristics to MORB, are produced during the rifting and spreading stages by the upwelling of the asthenospheric mantle due to the induced mantle flow in the mantle wedge (e.g., Jurdy and Stefanick, 1983). Although the East Sea opening ceased during the Miocene, the low-velocity zone is still observed in the upper mantle beneath the Ulleung basin, indicating that upwelling of the hot upper mantle is ongoing (e.g., Chen et al., 2017; Song et al., 2020; Wei et al., 2012). Moreover, several studies have proposed that the upwelling of the asthenospheric mantle is related to the Cenozoic volcanism in the Korean peninsula and northeastern China (Chen et al., 2017; Wei et al., 2012 and references therein).

There are many back-arc basins in the western Pacific region (Fig. 1a) (e.g., East Sea, Okinawa Trough, Mariana Trough, Manus basin, North Fiji basin, and Lau basin), and helium isotope compositions have been reported for samples of basaltic glasses or hydrothermal fluids (Fig. 10a). In general, the MORB-like $^{3}He/^{4}He$ ratios (8 ± 1 Ra) were observed in the most basaltic glass samples from the back-arc basins that have undergone the seafloor spreading stage, such as the south Mariana Trough, the central and southern Lau basins, and the southern Okinawa Trough (Fig. 10a). Exceptionally, high $^{3}He/^{4}He$ values (> 9 Ra) are shown in the Manus and northwestern Lau basins, which means that there is an influence of the lower mantle plume (Fig. 10a). In addition, most BABBs are sub-alkaline and show similar properties of major and trace elements between the IAB and MORB types derived from the asthenospheric mantle wedge (Fig. 10b–e). Therefore, the BABB glass samples in the areas where the seafloor spreading has already occurred would have originated from the asthenosphere. Compared to other BABBs, the DU basalts are more alkaline with enriched trace element patterns like OIB and have lower $^{3}He/^{4}He$ ratios than the MORB value (Fig. 10a–e). Another difference is that

there is no evidence of seafloor spreading in the Ulleung basin (e.g., Jolivet and Tamaki, 1992; Tamaki, 1988). The East Sea opening began in the late Eocene to the Oligocene, but the Ulleung basin was not sufficiently opened due to the subduction of the Philippine Sea plate in the Middle Miocene (15 to 12 Ma) (e.g., Jolivet and Tamaki, 1992; Tamaki, 1988). Accordingly, unlike the Yamato and Japan basins in the East Sea, no clue has been found for the formation of the oceanic crust in the Ulleung basin (Hirahara et al., 2015; Tamaki et al., 1992). The basalts and hydrothermal fluids found in the middle Okinawa Trough, where the continental rifting has occurred during the back-arc basin opening, have lower $^{3}He/^{4}He$ ratios ranging from 1.7 to 6.5 Ra (Ishibashi et al., 1995; Yu et al., 2016), suggesting the influence of the continental lithosphere. Therefore, the SCLM is suggested to exist as a major component of the Ulleung basin, where the oceanic lithosphere does not appear, resulting in the DU volcanic rocks with compositions similar to continental basalts rather than the typical BABBs.

Many studies suggested that lithosphere-asthenosphere interaction plays an important role in continental basalt formation (e.g., Konrad et al., 2016; Tang et al., 2006; Thompson and Gibson, 1994). Since the DU basalts have similar geochemical characteristics to continental basalts, we tested the interaction between lithosphere and asthenosphere for the DU magmas. The lithospheric and asthenospheric contributions to the DU basalt formation were investigated using a two-component mixing model in terms of helium isotopes and trace elements. We supposed conditions under which the lithosphere-derived melts mixed with asthenosphere-derived melts. It was assumed that the end-member composition of the asthenospheric melt coincided with popping rocks (Jones et al., 2019) for trace elements and 8 Ra for helium isotopes. As mentioned in section 5.2.4, the lithosphere was assumed to be a metasomatized mantle component, thus being considered to exhibit enriched geochemical features (e.g., high La/Yb and Nb/Y ratios). Therefore, we inferred that the end-member of the lithospheric melt is similar to the most extremely enriched (highest) trace element ratios of the DU basalts. The

helium isotope range was applied from 4.5 to 7.7 Ra based on results obtained from basalts and xenoliths in East Asia (this study; Chen et al., 2007; Kim et al., 2005). According to this model (Fig. 11), most of the DU samples are plotted between two mixing lines and represent less than 10% of the asthenospheric contribution, except for UD-1 (15%). This trend indicates that the dominant lithospheric melts were affected to some extent by the asthenospheric melts during DU magma generation. Additionally, the SCLM beneath the DU region seems to have lower $^{3}He/^{4}He$ ratios (4.5–6 Ra), which is close to the lower limit of the previously reported East Asian xenoliths (Chen et al., 2007; Kim et al., 2005). We also plotted the compositions of the Cenozoic basalts from eastern NCC (from Xu et al., 2014) in Fig. 11, following the trend towards the upper mixing line. This probably means that the SCLM beneath eastern NCC has higher $^{3}He/^{4}He$ values than the DU region, which can imply heterogeneity in the lithospheric mantle in East Asia. In Fig. 11b, one sample (Xu et al., 2014) taken from the eastern NCC basalts shows a higher contribution (> 30%) of the asthenosphere, which indicates a different degree of mixing in each region. Therefore, these mixing trends using helium isotopes and trace elements demonstrate that the Cenozoic basalts from the DU and NE China regions could be formed by varying degrees of lithosphere-asthenosphere interaction.

The low-velocity zone is observed from the upper mantle to the crust levels beneath both of DU by *P*- and *S*- wave seismic-tomography (Fig. 12a-d; Song et al., 2020). Kim et al. (2003) and references therein noted that the Ulleung basin has a higher mantle temperature or extensive magmatic underplating in the lower crust, indicating the presence of hot mantle upwelling. Moreover, it is suggested that the Cenozoic volcanic activities in East Asia are due to the asthenospheric upwelling resulting in the lithospheric thinning (Liu et al., 2019 and references therein). Also, in other regions (e.g., East Africa, Rio Grande, and Eger) where continental basalts are found, it is specified that the interaction between the asthenosphere and the lithosphere is the main mechanism of the formation of alkaline basalts (Thompson and

Gibson, 1994). In particular, in the case of East Africa, despite the presence of the lower mantle plume, the helium isotope ratios in the rock and fluid samples appear within the SCLM range in most regions due to the influence of the lithosphere (Lee et al., 2017 and references therein). Therefore, the DU basalts should be regarded as continental basalts, and such a large influence of the lithospheric mantle is clearly distinguished from the causes of the formation of other BABBs. Through this point, our results confirmed that the Ulleung basin did not completely form oceanic rifts, as seen in the Yamato and Japan basins, and remained in the lithosphere stretching phase as proposed in previous studies (e.g., Jolivet and Tamaki, 1992; Tamaki, 1988).

6. Conclusions

The DU volcanic islands formed in the East Sea as a part of the Cenozoic intraplate volcanism prevalent in East Asia. We report the first results of helium isotope compositions of DU mafic volcanic rocks to investigate the magma source. The rock samples selected from the drilling core and submarine/subaerial sites of the DU volcanoes have a Mg# range of 29.2 to 58.3, and show trace element patterns similar to OIBs. The $^{3}He/^{4}He$ ratios range from 5.7 to 5.9 Ra for Dokdo and 4.5 to 6.0 Ra for Ulleungdo, respectively. The range of our helium isotope ratios is similar to previously reported $^{3}He/^{4}He$ ratios of hornblendes (5.9–6.4 Ra) contained in the Ulleungdo felsic plutonic rocks (Kim et al., 2008). The uniform $^{3}He/^{4}He$ ratios of olivine, clinopyroxene, and hornblende indicate that volatile compositions did not change significantly in the formation of the DU volcanoes from 2.47 to 0.12 Ma without degassing effects or crustal contamination. Moreover, the $^{3}He/^{4}He$ ratios are similar to the SCLM range of East Asia (4.6 to 7.7 Ra), indicating that the depleted asthenosphere or the lower mantle plume might not be the direct source of the DU magmas. Also, there is no evidence that the DU magmas were influenced by subduction-derived components or the HIMU mantle source. On the other hand, the DU volcanic rocks have similar properties to the global continental basalts, suggesting that

the SCLM contribution is major unlike basalts from other back-arc basins composed of the oceanic crust. In this respect, we support the suggestion that the extended SCLM still remains beneath the Ulleung basin. A two-component mixing model estimates that the DU basalts and other Cenozoic basalts from northeastern China show mixing trends between the metasomatized lithospheric melts and the asthenospheric melts. In addition, the existence of low-velocity zones underneath East Asia, including the DU volcanoes, indicates that the magmas formed through the lithospheric melting due to the asthenospheric upwelling. Therefore, our study demonstrates that the enriched magma source for the DU volcanoes is primarily contributed by SCLM, and that the lithosphere-asthenosphere interaction resulted in the Cenozoic magmatism in East Asia, like other continental basalts in the world.

Declaration of interests

The authors declare that there is no conflict of interest regarding the publication of this paper.

Acknowledgments

This study was supported by the Ministry of Oceans and Fisheries, Korea—Sustainable Research and Development of Dokdo (PG51650) and the National Research Foundation of Korea (NRF-2019R1G1A1002297). We thank the staff members of Onnuri R/V for collecting the dredge samples. We are grateful to the administrative staff of the East Sea Research Institute, Korea Institute of Ocean Science and Technology (KIOST). We thank Xian-Hua Li for handling our manuscript as an editor. We also appreciate two anonymous reviewers for constructive comments to improve our manuscript.

References

Allan, J.F., Gorton, M.P., 1992. Geochemistry of igneous rocks from Legs 127 and 128, Sea of Japan. Proc., Sci. results. 127/128, 905–929.

https://doi.org/10.2973/odp.proc.sr.127128.208.1992

Baxter, E.F., 2010. Diffusion of noble gases in minerals. Rev. Mineral. Geochemistry 72, 509–557. https://doi.org/10.2138/rmg.2010.72.11

Brenna, M., Price, R., Cronin, S.J., Smith, I.E.M., Sohn, Y.K., Kim, G., Maas, R., 2014. Final magma storage depth modulation of explosivity and trachyte-phonolite genesis at an intraplate volcano: A case study from Ulleung Island, South Korea. J. Petrol. 55, 709–747. https://doi.org/10.1093/petrology/egu004

Carracedo, A., Rodés, Smellie, J. L., Stuart, F. M., 2019. Episodic erosion in West Antarctica inferred from cosmogenic ^{3}He and ^{10}Be in olivine from Mount Hampton. Geomorphology, 327, 438–445. https://doi.org/10.1016/j.geomorph.2018.11.019

Chen, C., Zhao, D., Tian, Y., Wu, S., Hasegawa, A., Lei, J., Park, J.H., Kang, I.B., 2017. Mantle transition zone, stagnant slab and intraplate volcanism in Northeast Asia. Geophys. J. Int. 209, 68–85. https://doi.org/10.1093/gji/ggw491

Chen, S.S., Liu, J.Q., Chen, S.S., Guo, Z.F., Sun, C.Q., 2015. Variations in the geochemical structure of the mantle wedge beneath the northeast Asian marginal region from pre- to post-opening of the Japan Sea. Lithos 224–225, 324–341. https://doi.org/10.1016/j.lithos.2015.03.008

Chen, S.S., Lee, S.G., Lee, T.J., Lee, Y.S., Liu, J.Q., 2018. Multi-stage magmatic plumbing system of the volcano: A case study from Ulleung Island, South Korea. Lithos 314–315, 201–215. https://doi.org/10.1016/j.lithos.2018.05.028

Chen, Y., Zhang, Y., Graham, D., Su, S., Deng, J., 2007. Geochemistry of Cenozoic basalts and mantle xenoliths in Northeast China. Lithos 96, 108–126. https://doi.org/10.1016/j.lithos.2006.09.015

Choi, S.H., Kwon, S.T., Mukasa, S.B., Sagong, H., 2005. Sr–Nd–Pb isotope and trace element systematics of mantle xenoliths from Late Cenozoic alkaline lavas, South Korea. Chem. Geol. 221, 40–64. https://doi.org/10.1016/j.chemgeo.2005.04.008

Choi, S.H., Mukasa, S.B., Kwon, S.T., Andronikov, A. V., 2006. Sr, Nd, Pb and Hf isotopic compositions of late Cenozoic alkali basalts in South Korea: Evidence for mixing between the two dominant asthenospheric mantle domains beneath East Asia. Chem. Geol. 232, 134–151. https://doi.org/10.1016/j.chemgeo.2006.02.014

Day, J.M.D., Barry, P.H., Hilton, D.R., Burgess, R., Pearson, D.G., Taylor, L.A., 2015. The helium flux from the continents and ubiquity of low-$^{3}He/^{4}He$ recycled crust and lithosphere. Geochim. Cosmochim. Acta 153, 116–133. https://doi.org/10.1016/j.gca.2015.01.008

Dodson, A., DePaolo, D.J., Kennedy, B.M., 1998. Helium isotopes in lithospheric mantle: Evidence from Tertiary basalts of the western USA. Geochim. Cosmochim. Acta 62, 3775–3787. https://doi.org/10.1016/S0016-7037(98)00267-1

Elsasser, W.M., 1971. Sea-floor spreading as thermal convection. J. Geophys. Res. 76, 1101–1112.

Fitton, J.G., Saunders, A.D., Norry, M.J., Hardarson, B.S., Taylor, R.N., 1997. Thermal and chemical structure of the Iceland plume. Earth Planet. Sci. Lett. 153, 197–208. https://doi.org/10.1016/s0012-821x(97)00170-2

Frey, F.A., Green, D.H., Roy, S.D., 1978. Integrated models of basalt petrogenesis: A study of quartz tholeiites to olivine melilitites from South Eastern Australia utilizing geochemical and experimental petrological data. J. Petrol. 19, 463–513. https://doi.org/10.1093/petrology/19.3.463

Gautheron, C., Moreira, M., 2002. Helium signature of the subcontinental lithospheric mantle. Earth Planet. Sci. Lett. 199, 39–47. https://doi.org/10.1016/S0012-821X(02)00563-0

Graham, D.W., Humphris, S.E., Jenkins, W.J., Kurz, M.D., 1992. Helium isotope geochemistry of some volcanic rocks from Saint Helena. Earth Planet. Sci. Lett. 110, 121–131. https://doi.org/10.1016/0012-821X(92)90043-U

Graham, D.W., 2002. Noble gas isotope geochemistry of mid-ocean ridge and ocean island basalts: Characterization of mantle source reservoirs. Rev. Mineral. Geochemistry 47, 247–317. https://doi.org/10.2138/rmg.2002.47.8

Halldórsson, S.A., Hilton, D.R., Scarsi, P., Abebe, T., Hopp, J., 2014. A common mantle plume source beneath the entire East African Rift System revealed by coupled helium-neon systematics. Geophys. Res. Lett. 41, 2304–2311. https://doi.org/10.1002/2014GL059424

Hanyu, T., Kaneoka, I., 1997. The uniform and low $^{3}He/^{4}He$ ratios of HIMU basalts as evidence for their origin as recycled materials. Nature 390, 273–276. https://doi.org/10.1038/36835

Harrison, D., Barry, T., Turner, G., 2004. Possible diffusive fractionation of helium isotopes in olivine and clinopyroxene phenocrysts. Eur. J. Mineral. 16, 213–220. https://doi.org/10.1127/0935-1221/2004/0016-0213

Hilton, D.R., Hammerschmidt, K., Loock, G., Friedrichsen, H., 1993. Helium and argon isotope systematics of the central Lau Basin and Valu Fa Ridge: Evidence of crust/mantle interactions in a back-arc basin. Geochim. Cosmochim. Acta 57, 2819–2841. https://doi.org/10.1016/0016-7037(93)90392-A

Hilton, D.R., Fischer, T.P., Marry, B., 2002. Noble gases and volatile recycling at subduction

zones. Rev. Mineral. Geochemistry 47, 319–370. https://doi.org/10.2138/rmg.2002.47.9

Hirahara, Y., Kimura, J.-I., Senda, R., Miyazaki, T., Kawabata, H., Takahashi, T., Chang, Q., Vaglarov, B.S., Sato, T., Kodaira, S., 2015. Geochemical variations in Japan Sea back-arc basin basalts formed by high-temperature adiabatic melting of mantle metasomatized by sediment subduction components. Geochemistry, Geophys. Geosystems 16, 1324–1347. https://doi.org/10.1002/2015GC005720

Hofmann, A.W., Jochum, K.P., Seufert, M., White, W.M., 1986. Nb and Pb in oceanic basalts: new constraints on mantle evolution. Earth Planet. Sci. Lett. 79, 33–45. https://doi.org/10.1016/0012-821X(86)90038-5

Ikeda, Y., Nagao, K., Stern, R.J., Yuasa, M., Newman, S., 1998. Noble gases in pillow basalt glasses from the northern Mariana Trough back-arc basin. Isl. Arc 7, 471–478. https://doi.org/10.1111/j.1440-1738.1998.00204.x

Ishibashi, J., Sano, Y., Wakita, H., Gamo, T., Tsutsumi, M., Sakai, H., 1995. Helium and carbon geochemistry of hydrothermal fluids from the Mid-Okinawa Trough Back Arc Basin, southwest of Japan. Chem. Geol. 123, 1–15. https://doi.org/10.1016/0009-2541(95)00051-M

Ishizuka, O., Yuasa, M., Tamura, Y., Shukuno, H., Stern, R.J., Naka, J., Joshima, M., Taylor, R.N., 2010. Migrating shoshonitic magmatism tracks Izu-Bonin-Mariana intra-oceanic arc rift propagation. Earth Planet. Sci. Lett. 294, 111–122. https://doi.org/10.1016/j.epsl.2010.03.016

Jenner, F.E., Arculus, R.J., Mavrogenes, J.A., Dyriw, N.J., Nebel, O., Hauri, E.H., 2012. Chalcophile element systematics in volcanic glasses from the northwestern Lau Basin. Geochemistry, Geophys. Geosystems 13. https://doi.org/10.1029/2012GC004088

Jolivet, L., Tamaki, K., 1992. Neogene kinematics in the Japan Sea region and volcanic activity of the northeast Japan Arc. Proc., Sci. results, ODP, Legs 127/128, Japan Sea 127, 1311–1331. https://doi.org/10.2973/odp.proc.sr.127128.239.1992

Jones, M.R., Wanless, V.D., Soule, S.A., Kurz, M.D., Mittelstaedt, E., Fornari, D.J., Curtice, J., Klein, F., Le Roux, V., Brodsky, H., Péron, S., Schwartz, D.M., 2019. New constraints on mantle carbon from Mid-Atlantic Ridge popping rocks. Earth Planet. Sci. Lett. 511, 67–75. https://doi.org/10.1016/j.epsl.2019.01.019

Jurdy, D.M., Stefanick, M., 1983. Flow models for back-arc spreading. Tectonophysics 99, 191–206. https://doi.org/10.1016/0040-1951(83)90102-6

Kim, H.J., Jou, H.T., Cho, H.M., Bijwaard, H., Sato, T., Hong, J.K., Yoo, H.S., Baag, C.-E., 2003. Crustal structure of the continental margin of Korea in the East Sea (Japan Sea) from deep seismic sounding data: evidence for rifting affected by the hotter than normal mantle. Tectonophysics 364, 25–42. https://doi.org/10.1016/S0040-1951(03)00048-9

Kim, K.H., Tanaka, T., Nagao, K., Jang, S.K., 1999. Nd and Sr isotopes and in K-Ar ages of the Ulreungdo the East Sea, South Korea alkali volcanic rocks. Geochem. J. 33, 317.

Kim, K.H., Nagao, K., Tanaka, T., Sumino, H., Nakamura, T., Okuno, M., Lock, J.B., Youn, J.S., Song, J., 2005. He-Ar and Nd-Sr isotopic compositions of ultramafic xenoliths and host alkali basalts from the Korean peninsula. Geochem. J. 39, 341–356. https://doi.org/10.2343/geochemj.39.341

Kim, K.H., Nagao, K., Sumino, H., Tanaka, T., Hayashi, T., Nakamura, T., Lee, J.I., 2008. He–Ar and Nd–Sr isotopic compositions of late Pleistocene felsic plutonic back arc basin rocks from Ulleungdo volcanic island, South Korea: Implications for the genesis of young

plutonic rocks in a back arc basin. Chem. Geol. 253, 180–195. https://doi.org/10.1016/j.chemgeo.2008.05.009

Kim, N.H., Song, Y.S., Park, K.H., Lee, H.S., 2009. SHRIMP U-Pb Zircon Ages of the Granite Gneisses from the Pyeonghae Area of the northeastern Yeongnam Massif (Sobaeksan Massif). Jour. Pet. Soc. Korea 18, 31–47 (in Korean with English abstract).

Kimura, J.I., Sakuyama, T., Miyazaki, T., Vaglarov, B.S., Fukao, Y., Stern, R.J., 2018. Plume-stagnant slab-lithosphere interactions: Origin of the late Cenozoic intra-plate basalts on the East Eurasia margin. Lithos 300–301, 227–249. https://doi.org/10.1016/j.lithos.2017.12.003

Klemme, S., Günther, D., Hametner, K., Prowatke, S., Zack, T., 2006. The partitioning of trace elements between ilmenite, ulvospinel, armalcolite and silicate melts with implications for the early differentiation of the moon. Chem. Geol. 234, 251–263. https://doi.org/10.1016/j.chemgeo.2006.05.005

Konrad, K., Graham, D.W., Thornber, C.R., Duncan, R.A., Kent, A.J.R., Al-Amri, A.M., 2016. Asthenosphere-lithosphere interactions in Western Saudi Arabia: Inferences from 3He/4He in xenoliths and lava flows from Harrat Hutaymah. Lithos 248–251, 339–352. https://doi.org/10.1016/j.lithos.2016.01.031

Le Bas, M.J., Le Maitre, R.W., Streckeisen, A., Zanettin, B., 1986. A chemical classification of volcanic rocks based on the total alkali-silica diagram. J. Petrol. 27, 745–750. https://doi.org/10.1093/petrology/27.3.745

Lee, H., Fischer, T.P., Muirhead, J.D., Ebinger, C.J., Kattenhorn, S.A., Sharp, Z.D., Kianji, G., Takahata, N., Sano, Y., 2017. Incipient rifting accompanied by the release of subcontinental lithospheric mantle volatiles in the Magadi and Natron basin, East Africa. J.

Volcanol. Geotherm. Res. 346, 118–133. https://doi.org/10.1016/j.jvolgeores.2017.03.017

Lee, J.I., Hur, S.D., Lee, M.J., Yoo, C.M., Park, B.K., Kim, Y., Kwon, M.S., Nagao, K., 2002. Petrology and Geochemistry of Dokdo Volcanic Rocks, East Sea. Ocean Polar Res. 24, 465–482 (in Korean with English abstract). https://doi.org/10.4217/OPR.2002.24.4.465

Liu, J., Cai, R., Pearson, D.G., Scott, J.M., 2019. Thinning and destruction of the lithospheric mantle root beneath the North China Craton: A review. Earth-Science Rev. 196, 102873. https://doi.org/10.1016/j.earscirev.2019.05.017

Lupton, J., Rubin, K.H., Arculus, R., Lilley, M., Butterfield, D., Resing, J., Baker, E., Embley, R., 2015. Helium isotope, C/^{3}He, and Ba-Nb-Ti signatures in the northern Lau Basin: Distinguishing arc, back-arc, and hotspot affinities. Geochemistry, Geophys. Geosystems 16, 1133–1155. https://doi.org/10.1002/2014GC005625

MacPherson, C.G., Hilton, D.R., Mattey, D.P., Sinton, J.M., 2000. Evidence for an ^{18}O-depleted mantle plume from contrasting ^{18}O/^{16}O ratios of back-arc lavas from the Manus Basin and Mariana Trough. Earth Planet. Sci. Lett. 176, 171–183. https://doi.org/10.1016/S0012-821X(00)00002-9

Matsuda, J., Matsumoto, T., Sumino, H., Nagao, K., Yamamoto, J., Miura, Y., Kaneoka, I., Takahata, N., Sano, Y., 2002. The ^{3}He/^{4}He ratio of new internal He Standard of Japan (HESJ). Geochem. J. 36, 191–195. https://doi.org/10.2343/geochemj.36.191

Nakamura, E., Campbell, I.H., McCulloch, M.T., Sun, S.S., 1989. Chemical geodynamics in a back arc region around the Sea of Japan: implications for the genesis of alkaline basalts in Japan, Korea, and China. J. Geophys. Res. 94, 4634–4654. https://doi.org/10.1029/JB094iB04p04634

Nardini, I., Armienti, P., Rocchi, S., Dallai, L., Harrison, D., 2009. Sr-Nd-Pb-He-O Isotope

and Geochemical Constraints on the Genesis of Cenozoic Magmas from the West Antarctic Rift. J. Petrol. 50, 1359–1375. https://doi.org/10.1093/petrology/egn082

Nishio, Y., Sasaki, S., Gamo, T., Hiyagon, H., Sano, Y., 1998. Carbon and helium isotope systematics of North Fiji Basin basalt glasses: Carbon geochemical cycle in the subduction zone. Earth Planet. Sci. Lett. 154, 127–138. https://doi.org/10.1016/s0012-821x(97)00187-8

Obayashi, M., Yoshimitsu, J., Nolet, G., Fukao, Y., Shiobara, H., Sugioka, H., Miyamachi, H., Gao, Y., 2013. Finite frequency whole mantle P wave tomography: Improvement of subducted slab images. Geophys. Res. Lett. 40, 5652–5657. https://doi.org/10.1002/2013GL057401

Putirka, K.D., 2008. Thermometers and barometers for volcanic systems. Rev. Mineral. Geochemistry 69, 61–120. https://doi.org/10.2138/rmg.2008.69.3

Qian, S.P., Ren, Z.Y., Zhang, L., Hong, L.B., Liu, J.Q., 2015. Chemical and Pb isotope composition of olivine-hosted melt inclusions from the Hannuoba basalts, North China Craton: Implications for petrogenesis and mantle source. Chem. Geol. 401, 111–125. https://doi.org/10.1016/j.chemgeo.2015.02.018

Rudnick, R.L., Gao, S., 2003. Composition of the Continental Crust. Treatise on Geochemistry, 1–64. https://doi.org/10.1016/B0-08-043751-6/03016-4

Sakuyama, T., Tian, W., Kimura, J.I., Fukao, Y., Hirahara, Y., Takahashi, T., Senda, R., Chang, Q., Miyazaki, T., Obayashi, M., Kawabata, H., Tatsumi, Y., 2013. Melting of dehydrated oceanic crust from the stagnant slab and of the hydrated mantle transition zone: Constraints from Cenozoic alkaline basalts in eastern China. Chem. Geol. 359, 32–48. https://doi.org/10.1016/j.chemgeo.2013.09.012

Sakuyama, T., Nagaoka, S., Miyazaki, T., Chang, Q., Takahashi, T., Hirahara, Y., Senda, R., Itaya, T., Kimura, J., Ozawa, K., 2014. Melting of the uppermost metasomatized asthenosphere triggered by fluid fluxing from ancient subducted sediment: Constraints from the quaternary basalt lavas at Chugaryeong Volcano, Korea. J. Petrol. 55, 499–528. https://doi.org/10.1093/petrology/egt074

Shaw, A.M., Hilton, D.R., Macpherson, C.G., Sinton, J.M., 2004. The CO_2-He-Ar-H_2O systematics of the Manus back-arc basin: Resolving source composition from degassing and contamination effects. Geochim. Cosmochim. Acta 68, 1837–1855. https://doi.org/10.1016/j.gca.2003.10.015

Shim, S.H., Im, J.H., Jang, Y.D., Choo, C.O., Park, B.J., Kim, J.H., 2010. Petrological Characteristics and Origin of Volcaniclasts within the Massive Tuff Breccia Formation from Dokdo Island, Korea. J. Petrol. Soc. Korea 19, 141–156 (in Korean with English abstract).

Shinjo, R., Chung, S., Kato, Y., Kimura, M., 1999. Geochemical and Sr-Nd isotopic characteristics of volcanic rocks from the Okinawa Trough and Ryukyu Arc: Implications for the evolution of a young, intracontinental back arc basin. J. Geophys. Res. Solid Earth 104, 10591–10608.

Shuto, K., Nohara-Imanaka, R., Sato, M., Takahashi, T., Takazawa, E., Kawabata, H., Takanashi, K., Ban, M., Watanabe, N., Fujibayashi, N., 2015. Across-arc variations in geochemistry of Oligocene to Quaternary basalts from the NE Japan arc: Constraints on source composition, mantle melting and slab input composition. J. Petrol. 56, 2257–2294. https://doi.org/10.1093/petrology/egv073

Song, J.H., Kim, S., Rhie, J., 2020. Heterogeneous modification and reactivation of a craton

margin beneath the Korean Peninsula from teleseismic travel time tomography. Gondwana Res. 81, 475–489. https://doi.org/10.1016/j.gr.2019.11.016

Song, Y.S., Park, K.H., Park, M.E., 1999. Major, Rare-Earth and Trace Geochemistry of Ulleungdo Volcanic rocks. J. Petrol. Soc. Korea 8, 57–70 (in Korean with English abstract).

Song, Y.S., Park, M.E., Par, K.H., 2006. Age and evolution of the volcanic rocks from Ulleung-do and Dok-do. J. Pet. Korea 15, 72–80 (in Korean with English abstract).

Staudacher, T., Allègre, C.J., 1988. Recycling of oceanic crust and sediments: the noble gas subduction barrier. Earth Planet. Sci. Lett. 89, 173–183. https://doi.org/10.1016/0012-821X(88)90170-7

Stuart, F.M., Ellam, R.M., Harrop, P.J., Fitton, J.G., Bell, B.R., 2000. Constraints on mantle plumes from the helium isotopic composition of basalts from the British Tertiary Igneous Province. Earth Planet. Sci. Lett. 177, 273–285. https://doi.org/10.1016/S0012-821X(00)00050-9

Stuart, F.M., Lass-Evans, S., Fitton, J.G., Ellam, R.M., 2003. High $^{3}He/^{4}He$ ratios in picritic basalts from Baffin Island and the role of a mixed reservoir in mantle plumes. Nature 424, 57–59. https://doi.org/10.1038/nature01711

Sun, S.S., McDonough, W.F., 1989. Chemical and isotopic systematics of oceanic basalts: Implications for mantle composition and processes. Geol. Soc. Spec. Publ. 42, 313–345. https://doi.org/10.1144/GSL.SP.1989.042.01.19

Tamaki, K., 1988. Geological structure of the Japan Sea and its tectonic implications. Bull. Geol. Surv. Japan 39, 269–365.

Tamaki, K., Suyehiro, K., Allan, J., Ingle, J.C., Pisciotto, K.A., 1992. Tectonic synthesis and implications of Japan Sea ODP drilling. Proc. Sci. results 127/128, 1333–1348. https://doi.org/10.2973/odp.proc.sr.127128.240.1992

Tang, Y.J., Zhang, H.F., Ying, J.F., 2006. Asthenosphere-lithospheric mantle interaction in an extensional regime: Implication from the geochemistry of Cenozoic basalts from Taihang Mountains, North China Craton. Chem. Geol. 233, 309–327. https://doi.org/10.1016/j.chemgeo.2006.03.013

Thompson, R.N., Gibson, S.A., 1994. Magmatic expression of lithospheric thinning across continental rifts. Tectonophysics 233, 41–68. https://doi.org/10.1016/0040-1951(94)90219-4

Uyeda, S., Kanamori, H., 1979. Back-arc opening and the mode of subduction. J. Geophys. Res. 84, 1049. https://doi.org/10.1029/jb084ib03p01049

Wang, Y., Zhao, Z.F., Zheng, Y.F., Zhang, J.J., 2011. Geochemical constraints on the nature of mantle source for Cenozoic continental basalts in east-central China. Lithos 125, 940–955. https://doi.org/10.1016/j.lithos.2011.05.007

Wei, W., Xu, J., Zhao, D., Shi, Y., 2012. East Asia mantle tomography: New insight into plate subduction and intraplate volcanism. J. Asian Earth Sci. 60, 88–103. https://doi.org/10.1016/j.jseaes.2012.08.001

Xu, Z., Zheng, Y.F., He, H.Y., Zhao, Z.F., 2014. Phenocryst He–Ar isotopic and whole-rock geochemical constraints on the origin of crustal components in the mantle source of Cenozoic continental basalt in eastern China. J. Volcanol. Geotherm. Res. 272, 99–110. https://doi.org/10.1016/j.jvolgeores.2014.01.001

Yamamoto, T., Hoang, N., 2009. Synchronous Japan Sea opening Miocene fore-arc

volcanism in the Abukuma Mountains, NE Japan: An advancing hot asthenosphere flow versus Pacific slab melting. Lithos 112, 575–590. https://doi.org/10.1016/j.lithos.2009.03.044

Yu, Z., Zhai, S., Guo, K., Zhou, Y., Zong, T., 2016. Helium isotopes in volcanic rocks from the Okinawa Trough-impact of volatile recycling and crustal contamination. Geol. J. 51, 376–386. https://doi.org/10.1002/gj.2794

Zou, H., Fan, Q., Yao, Y., 2008. U-Th systematics of dispersed young volcanoes in NE China: Asthenosphere upwelling caused by piling up and upward thickening of stagnant Pacific slab. Chem. Geol. 255, 134–142. https://doi.org/10.1016/j.chemgeo.2008.06.022

Table 1. Petrographical information of the DU volcanic rocks

Sample ID	**DD-1**	**DD-2**	**DD-3**	**DD-4**	**UD-1**	**UD-2**	**UD-3**	**UD-4**
Rock type	Basanite	Basalt	Trachy-basalt	Tephrite	Tephrite	trachy-basalt	Basaltic trachy-andesite	Basalt
mineral	clinopyroxene	clinopyroxene	olivine	olivine	olivine	clinopyroxene	clinopyroxene	clinopyroxene
Mode (vol. %)								
matrix	-	47.7	67.6	68.9	90.6	73	74.1	43.4
Ol	-	7.1	5.5	8	5.2	-	-	-
Cpx	-	43.2	13.3	12.4	0.1	13.9	4.3	4.8
Plg	-	2	13.3	10.7	2.5	2.8	17.7	3.4
Oxides	-	-	-	-	0.3	0.8	-	0.1
bubbles	-	-	0.3	0.1	1.3	9.4	1.4	48.3
Texture								
	porphyritic	porphyritic	porphyritic	porphyritic	porphyritic	porphyritic	porphyritic	porphyritic
	intergranular	intergranular	intergranular	intergranular	intergranular	intergranular	intergranular	intergranular
								Glassy and very vesicular
Remarks								
zoning	Various degrees of zoning on cpx and plg	Various degrees of zoning on cpx and plg	Various degrees of zoning on cpx and plg	Various degrees of zoning on cpx	Sieve texture and patch zoning in plg	Various degrees of zoning on cpx and plg	Various degrees of zoning on cpx and plg	Various degrees of zoning on cpx and plg

	Weakly normal and reverse zoning in ol	Weakly normal and reverse zoning in ol	Weakly normal and reverse zoning in ol	Weakly normal and reverse zoning in ol				
vesicles	Less vesicular	Less vesicular	Less vesicular	Less vesicular	Contain few irregular shape of vesicles	Contain many vesicles of varying sizes and irregular shapes	Contain vesicles of varying sizes and irregular shapes	Contain many circular vesicles with varying size
etc.	Most ol turned into iddingsite	Most ol turned into iddingsite		Poikilitic texture in cpx		Ophitic texture in cpx	Ophitic texture in cpx	
						Considerable size of glomerocryst of cpx and plg	Considerable size of glomerocryst of cpx and plg	

* The phenocryst mode of DD-1 was not obtained because there were no thin sections.

** Microphenocrysts which were not observed by unaided eyes were considered matrix components.

Table 2. Sampling information and whole-rock geochemistry

Location	**Dokdo**				**Ulleungdo**			
Sample Name	BH-4F	DD-02	DRD 1805-02	DRD 1805-09	URD 1801-02	UL-01	UL-02	URD 1901R-03
Sample ID	DD-1	DD-2	DD-3	DD-4	UD-1	UD-2	UD-3	UD-4
type	core	land	dredged	dredged	dredged	land	land	dredged
Latitude (ºN)	37.23795224	37.23913	37.30	37.30	37.56	37.482864	37.459725	37.351
Longitude (ºE)	131.8658103	131.8679	131.81	131.81	130.99	130.91224	130.857627	130.867
Rock type	Trachy-basalt	Basalt	Trachy-basalt	Tephrite	Trachy-basalt	Trachy-basalt	Basaltic trachy-andesite	Trachy-basalt
major element (wt. %)								
SiO2	44.9	47.1	48.5	47.5	47.4	47.8	51.3	46.5
Al2O3	15.2	15.5	16.0	17.1	16.0	17.6	18.5	15.7
Fe2O3	10.4	10.1	8.9	9.5	10.0	8.7	8.4	11.4
MnO	0.21	0.42	0.14	0.13	0.15	0.13	0.12	0.15
MgO	5.2	4.7	5.7	3.9	4.6	2.9	1.6	3.9
CaO	9.8	11.3	9.6	9.1	8.3	8.9	5.9	10.8
Na2O	2.3	3.3	3.0	3.3	3.5	2.7	5.1	2.6
K2O	3.1	1.5	3.3	3.8	3.3	3.3	2.1	2.4
TiO2	2.64	2.65	2.72	2.84	3.47	3.61	2.67	3.37
P2O5	0.8	0.7	0.8	1.2	1.3	0.9	1.1	0.6
LOI	5.3	2.5	0.0	1.5	0.8	3.4	3.1	2.4
Total	99.8	99.8	99.8	99.8	99.9	99.8	99.9	99.8
Mg#	52.2	50.9	58.3	47.1	50.6	42.7	29.2	42.8
CIPW norm (wt. %)								
Quartz	-	-	-	-	-	-	-	-

Plagioclase	36.3	45.4	37.3	36.3	41.0	51.2	67.6	41.7
Orthoclase	19.4	9.2	19.9	22.9	19.9	20.2	12.7	14.8
Nepheline	4.5	4.1	5.4	7.5	4.4	-	-	3.5
Diopside	18.8	24.2	18.5	14.2	11.9	10.8	0.7	22.5
Hypersthene	-	-	-	-	-	0.8	2.6	-
Olivine	13.7	10.1	11.8	10.7	12.8	7.7	8.4	9.5
Ilmenite	5.4	5.2	5.3	5.5	6.8	7.2	5.3	6.6
Apatite	2.0	1.8	2.0	2.9	3.2	2.1	2.6	1.4
Trace element (ppm)								
Sc	20.2	26.2	23.3	16.7	17.2	16.2	8.5	28.6
V	237	283	259	235	196	268	141	325
Cr	118.2	135.6	138.3	75.9	21.1	69.2	12.7	124.3
Co	72.5	200.7	33.2	175.7	19.2	165.2	47.3	47.4
Ni	117.5	81.7	48.7	42.7	14.2	45.5	11.4	48.5
Ga	18.0	20.3	22.4	20.2	21.4	23.2	18.2	25.7
Rb	47.8	36.5	69.4	70.8	52.8	65.2	44.6	44.5
Sr	876	870	992	962	1764	970	864	996
Y	18.0	21.9	23.9	21.5	30.8	25.5	19.5	25.9
Zr	263	288	351	324	278	341	265	338
Nb	67.6	81.7	102.6	92.4	76.1	82.5	67.4	80.1
Mo	3.35	2.73	5.12	4.12	3.55	3.47	2.34	9.54
Cs	0.45	1.85	0.80	0.78	0.51	0.62	0.75	0.68
Ba	795	877	972	943	6932	955	1100	969
La	59.2	63.6	74.1	78.1	69.5	65.4	62.8	49.3

Ce	108	115	137	139	137	120	113	96
Pr	11.5	12.5	14.7	14.8	15.9	13.2	12.1	11.4
Nd	42.2	46.2	53.0	53.6	62.5	50.8	45.1	44.0
Sm	6.68	7.61	8.29	8.26	10.99	8.53	7.25	8.60
Eu	2.23	2.45	2.73	2.67	5.23	2.93	2.60	2.79
Gd	5.35	6.25	6.66	6.37	9.48	7.35	5.84	7.15
Tb	0.75	0.84	0.91	0.84	1.24	1.05	0.74	1.04
Dy	3.93	4.54	4.82	4.86	6.24	5.13	4.01	5.27
Ho	0.66	0.83	0.88	0.86	1.14	0.99	0.75	0.97
Er	1.81	2.22	2.29	2.19	2.78	2.69	2.07	2.47
Tm	0.24	0.28	0.30	0.26	0.37	0.31	0.21	0.32
Yb	1.49	1.81	2.12	1.93	2.23	2.24	1.56	2.04
Lu	0.22	0.28	0.27	0.29	0.29	0.27	0.22	0.29
Hf	6.09	6.75	7.38	6.88	6.13	7.57	5.85	7.94
Ta	3.95	5.11	6.00	5.42	4.60	5.01	3.83	4.82
Pb	5.14	5.49	7.06	6.61	4.73	6.04	5.22	5.64
Th	8.17	9.37	10.43	10.76	7.09	9.64	7.59	7.83
U	1.82	2.16	2.07	2.41	1.80	1.80	0.92	1.88
Ce/Pb	21.0	20.9	19.4	21.1	29.0	19.9	21.7	17.0
Nb/U	37.2	37.8	49.6	38.3	42.2	45.9	73.4	42.6
La/Yb	39.9	35.2	34.9	40.4	31.2	29.2	40.4	24.1
Nb/Y	3.8	3.7	4.3	4.3	2.5	3.2	3.5	3.1

Table 3. Helium abundances, isotope compositions and U-Th contents of measured minerals

Sample ID	DD-1	DD-2	DD-3	DD-4	UD-1	UD-2	UD-3	UD-4
Rock type	Basanite	Basalt	Trachy-basalt	Tephrite	Tephrite	Trachy-basalt	Basaltic trachy-andesite	Basalt
mineral	clinopyroxene	clinopyroxene	olivine	olivine	olivine	clinopyroxene	clinopyroxene	clinopyroxene
mass (g)	0.375	0.359	0.312	0.362	0.344	0.34	0.321	0.424
^{4}He (10^{-9} ccSTP/g)	34.15	96.61	13.20	13.03	24.69	53.11	2.81	63.03
±	0.02	0.05	0.01	0.01	0.01	0.03	0.002	0.03
^{3}He (10^{-14} ccSTP/g)	27.80	76.68	10.97	10.42	16.23	44.48	1.91	43.60
±	1.72	4.74	0.68	0.64	1.00	2.75	0.12	2.70
$^{3}He/^{4}He$ (R/Ra)	5.8	5.7	5.9	5.7	4.7	6.0	4.5	4.9
1σ	0.2	0.1	0.3	0.3	0.3	0.2	0.9	0.1
U	0.01	0.02	-	-	-	0.01	0.02	0.02
±1σ	0.006	0.007	-	-	-	0.001	0.008	0.010
Th	0.12	0.09	-	-	-	0.11	0.15	0.10
±1σ	0.018	0.054	-	-	-	0.071	0.068	0.043

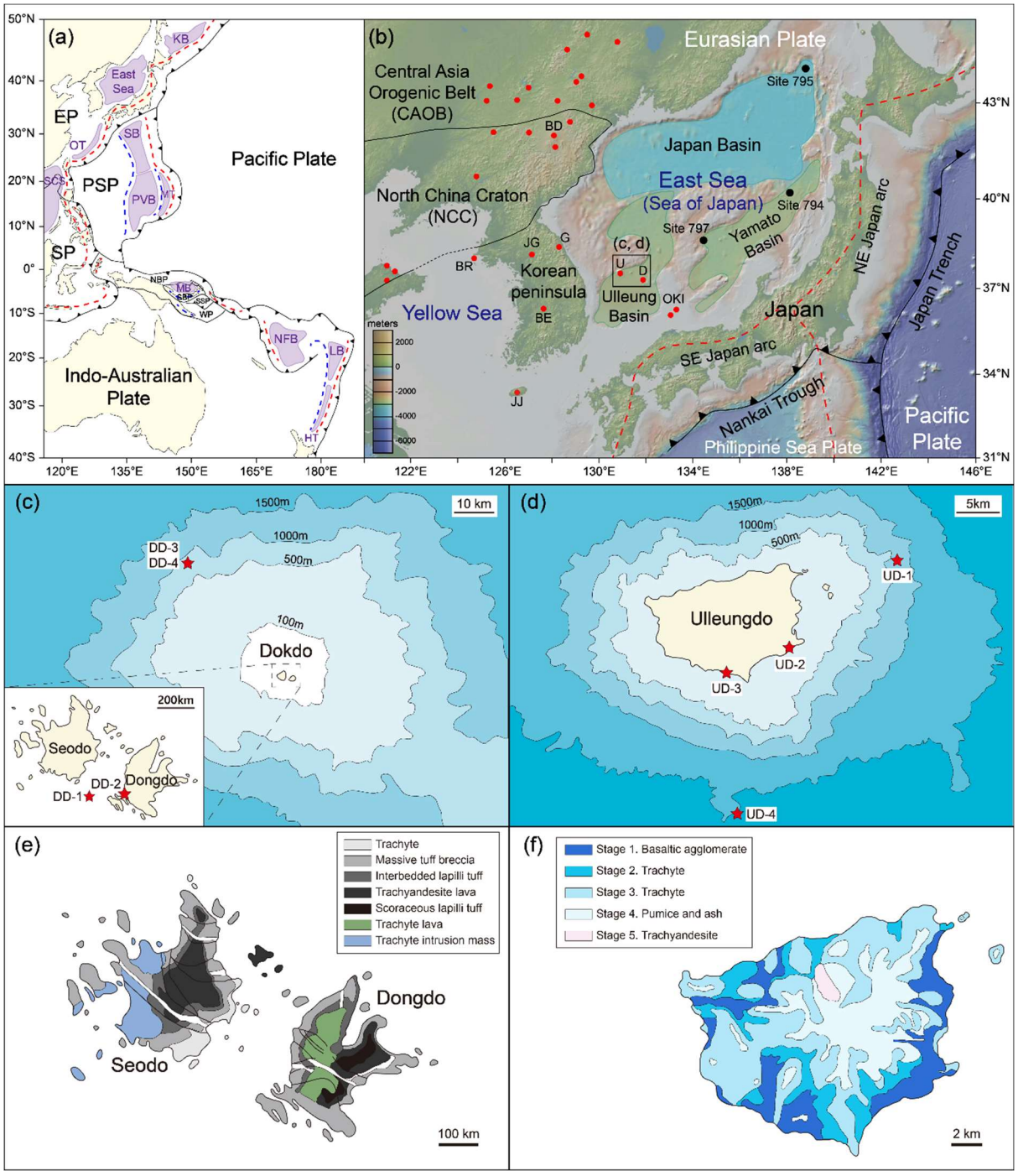

Fig. 1. (a) Simplified map of the western Pacific regions. Back-arc basins are shown as purple areas. Red dashed lines represent volcanic arc fronts, and blue dashed lines indicate inactive remnant volcanic arcs (EP = Eurasian plate, PSP = Philippine Sea Plate, SP = Sunda Plate, NBP = North Bismark Plate, SBP = South Bismark Plate, SSP = Solomon Sea Plate, WP = Woodlark Plate, KB = Kuril Basin, OT = Okinawa Trough, SCS = South China Sea, SB = Shikoku Basin, PVB = Parece Vela Basin, MT = Mariana Trough, MB = Manus Basin, NFB = North Fiji Basin,

LB = Lau Basin, HT = Havre Trough). (b) Geological map of the East Sea and adjacent areas (GeoMapApp 3.6.10). Red circles mean the Cenozoic volcanic fields of East Asia (BD = Mt. Baekdu/Changbaishan, BR = Beagnyeongdo, JG = Jeongok, G = Ganseong, BE = Boeun, U = Ulleungdo, D = Dokdo, JJ = Jeju). Red dashed line indicates active volcanic arc front. Blue area is the Japan basin consisting of the oceanic crust, and green areas are the Ulleung and Yamato basins mainly composed of the stretched continental lithosphere. (c) Dokdo and (d) Ulleungdo rock sample locations are shown on the contour maps as red stars. Geologic maps of (e) Dokdo and (f) Ulleungdo modified from Chen et al. (2018).

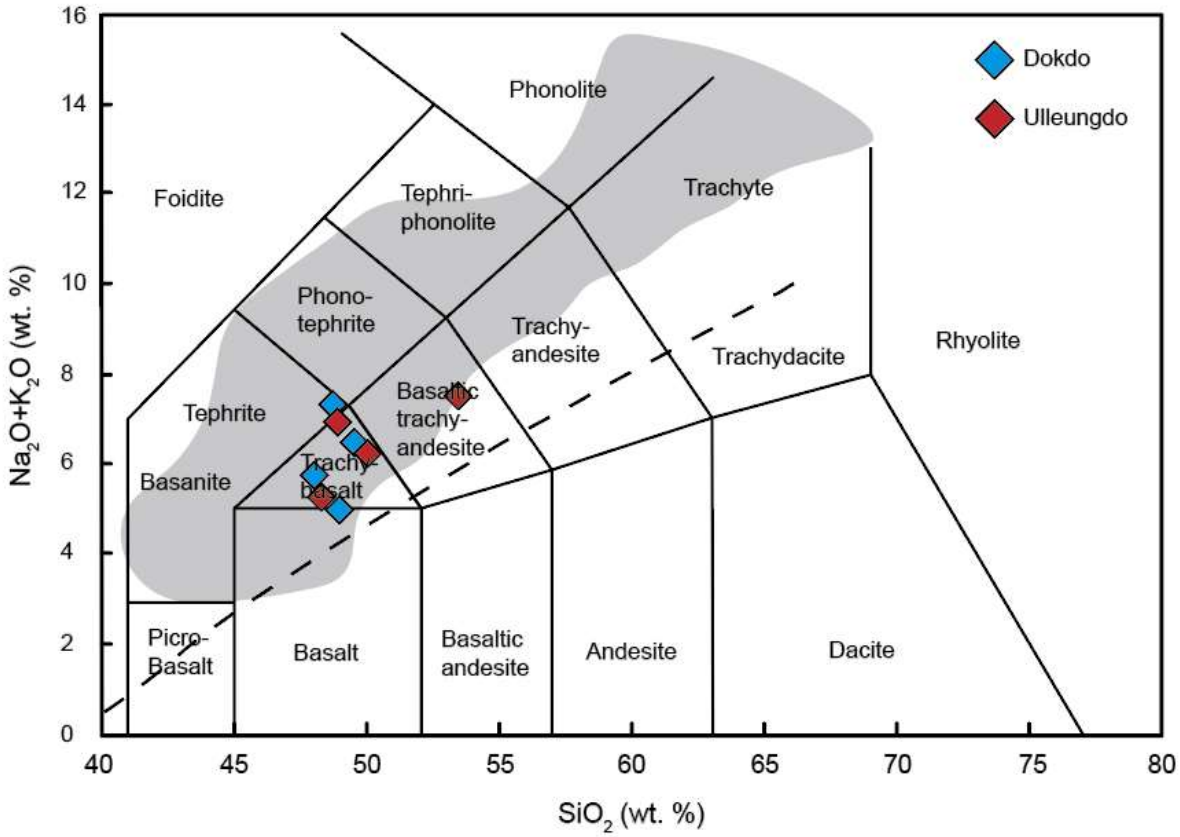

Fig. 2. Total alkali-silica (TAS) diagram (Le Bas et al., 1986) of the DU rock samples. Gray field indicates the range of the previously reported data of the DU volcanic rocks (Brenna et al., 2014; Chen et al., 2018; Lee et al., 2002; Shim et al., 2010; Song et al., 1999; unpublished data from Dokdo drilling core samples collected by KIOST in 2011). The symbols used in this diagram are all used identically in the following diagrams.

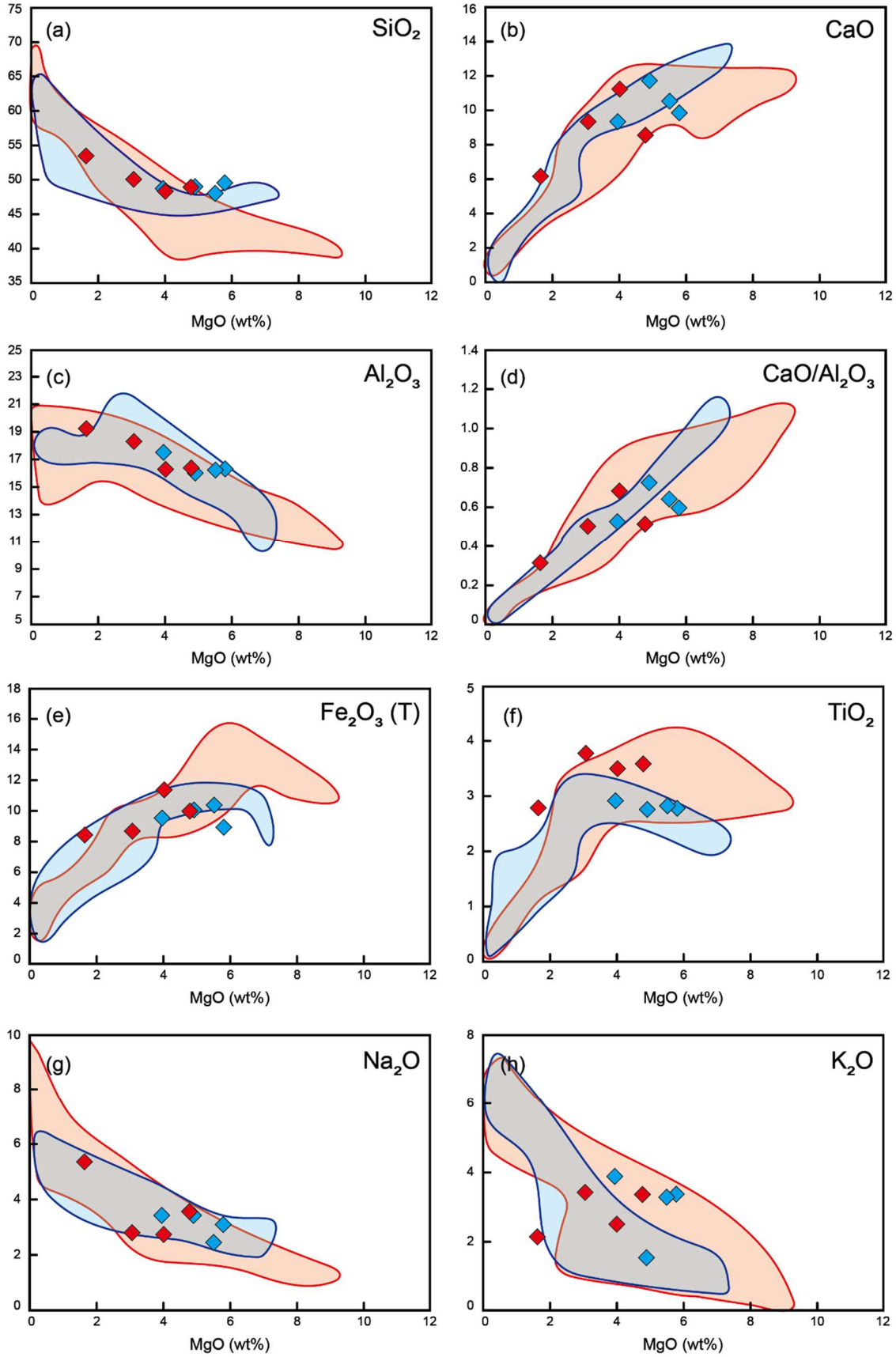
(a)
SiO2
(b)
CaO
(c)
Al2O3
(d)
CaO/Al2O3
(e)
Fe2O3 (T)
(f)
TiO2
(g)
Na2O
(h)
K2O
MgO (wt%)

895

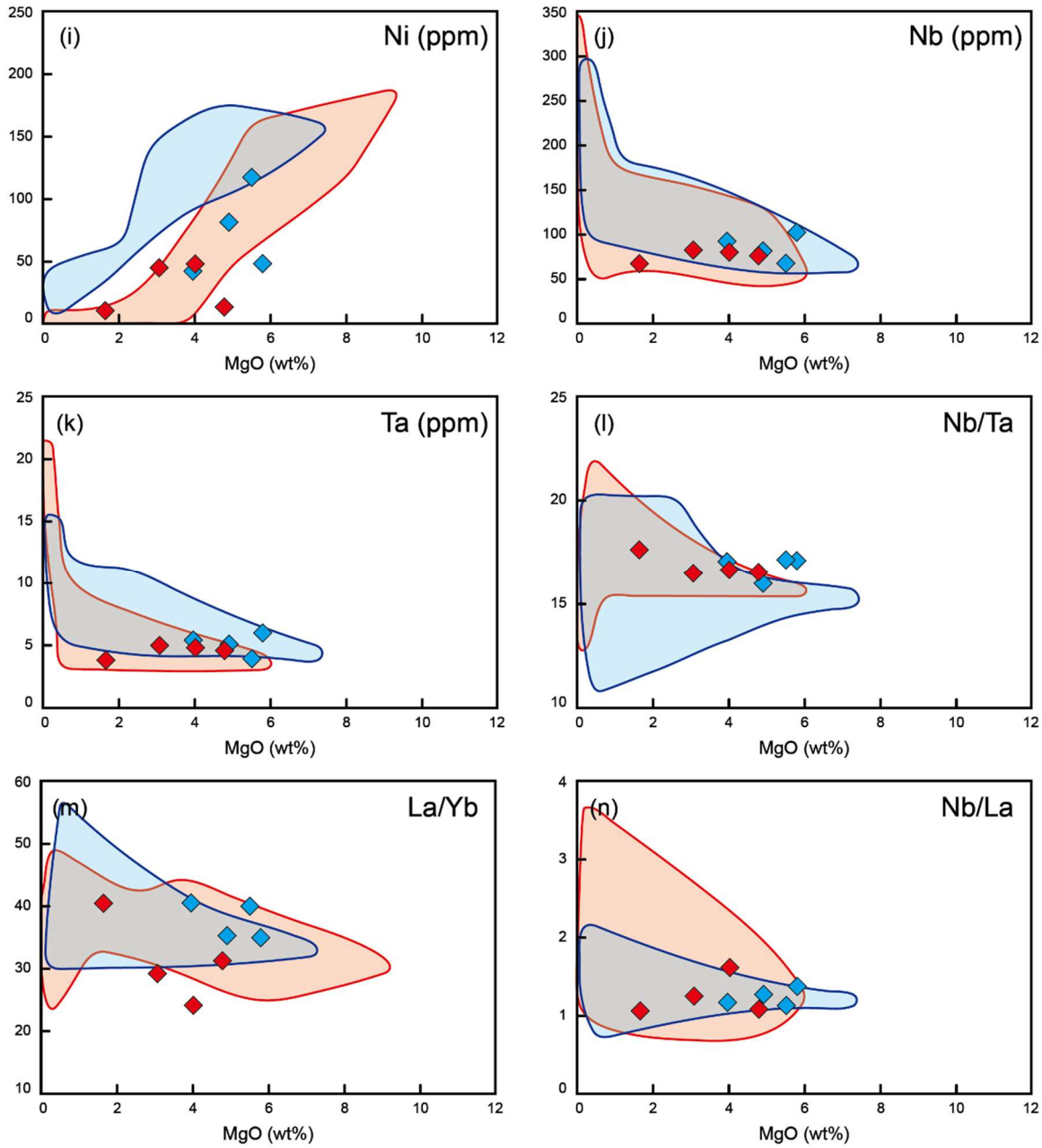

Fig. 3. Harker diagrams for the DU volcanic rocks. Blue and red areas indicate ranges of reference data of Dokdo and Ulleungdo, respectively. Reference data is shown in Fig. 2.

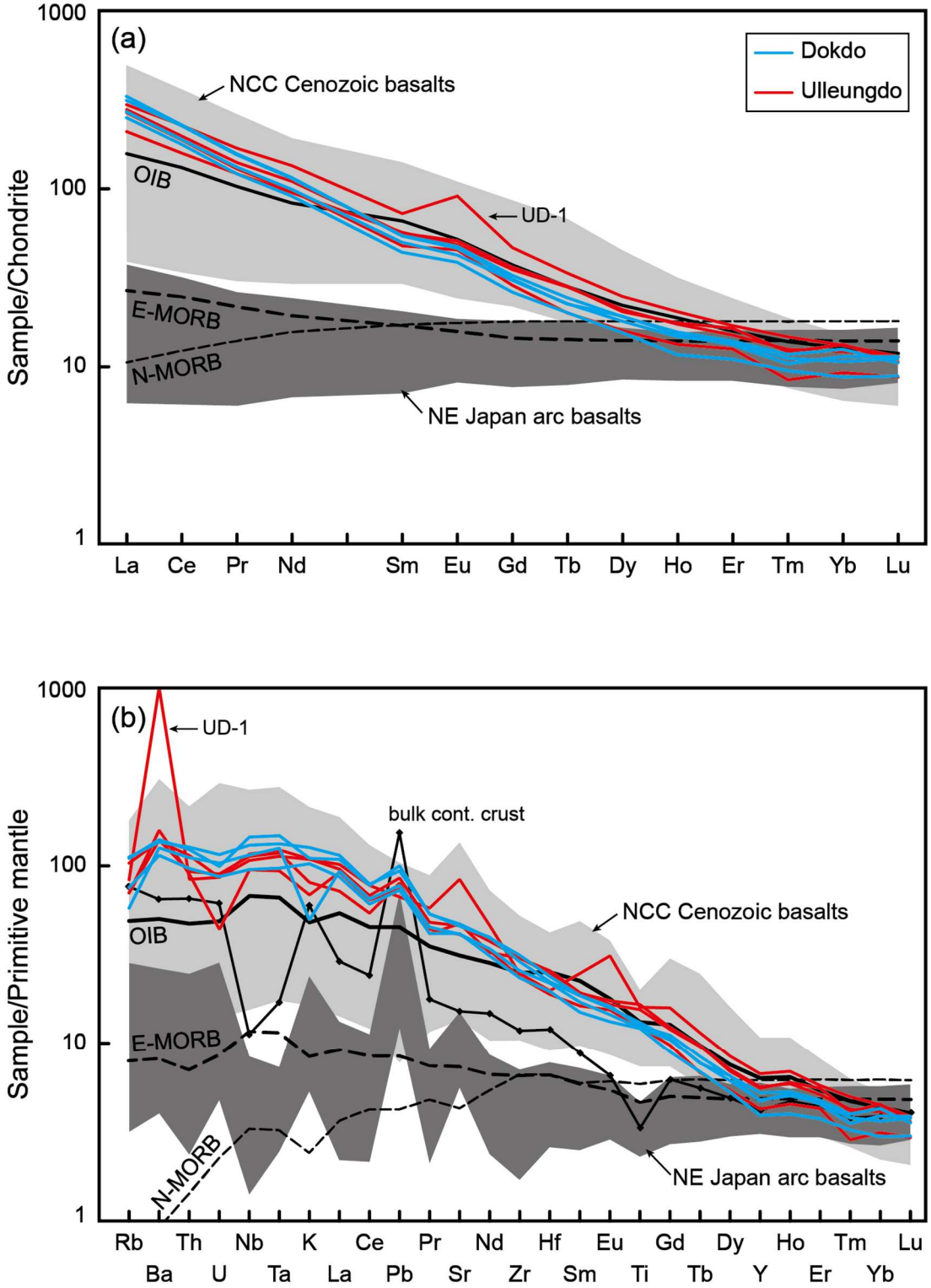

Fig. 4. (a) Chondrite-normalized REE patterns. (b) Primitive mantle-normalized multi-trace element spider diagram. Trace element concentrations of the chondrite, primitive mantle, N-MORB, E-MORB, and OIB components are from Sun and McDonough (1989). Trace element

concentrations of the bulk continental crust are from Rudnick and Gao (2003), and the NCC Cenozoic basalts are from Qian et al. (2015) and references therein.

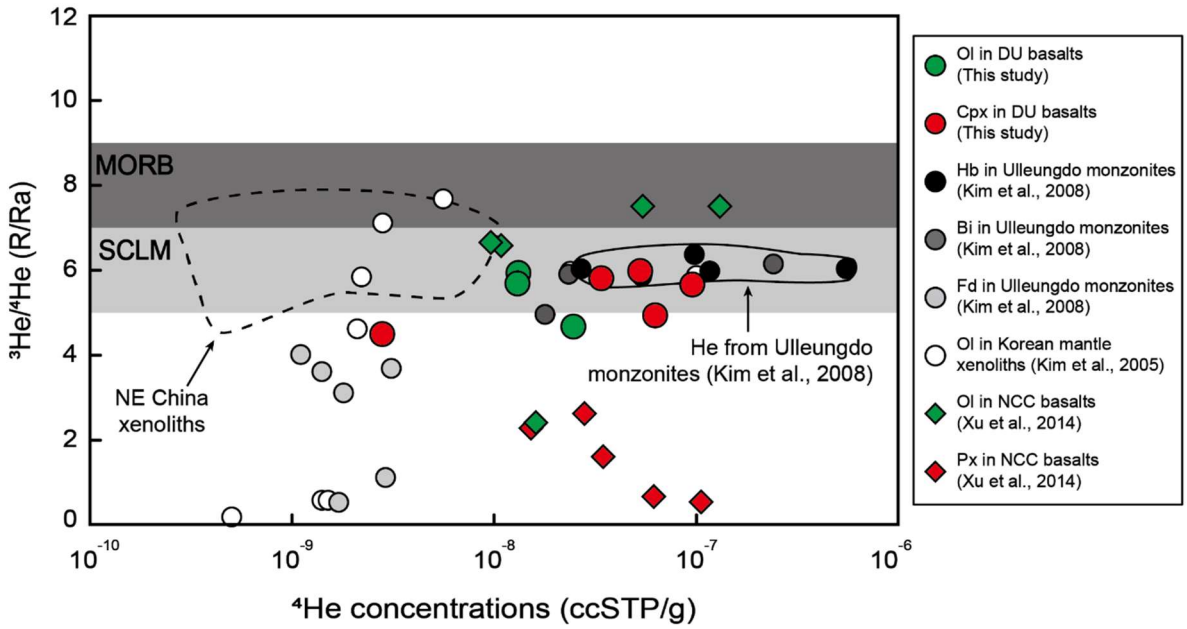

Fig. 5. Helium isotope ratios versus ^{4}He concentrations for the DU samples. The average MORB and SCLM values are from Graham (2002) and Gautheron and Moreira (2002), respectively. Helium isotope ratios of the NE China mantle xenoliths are from previous study using the crushing method (Chen et al., 2007).

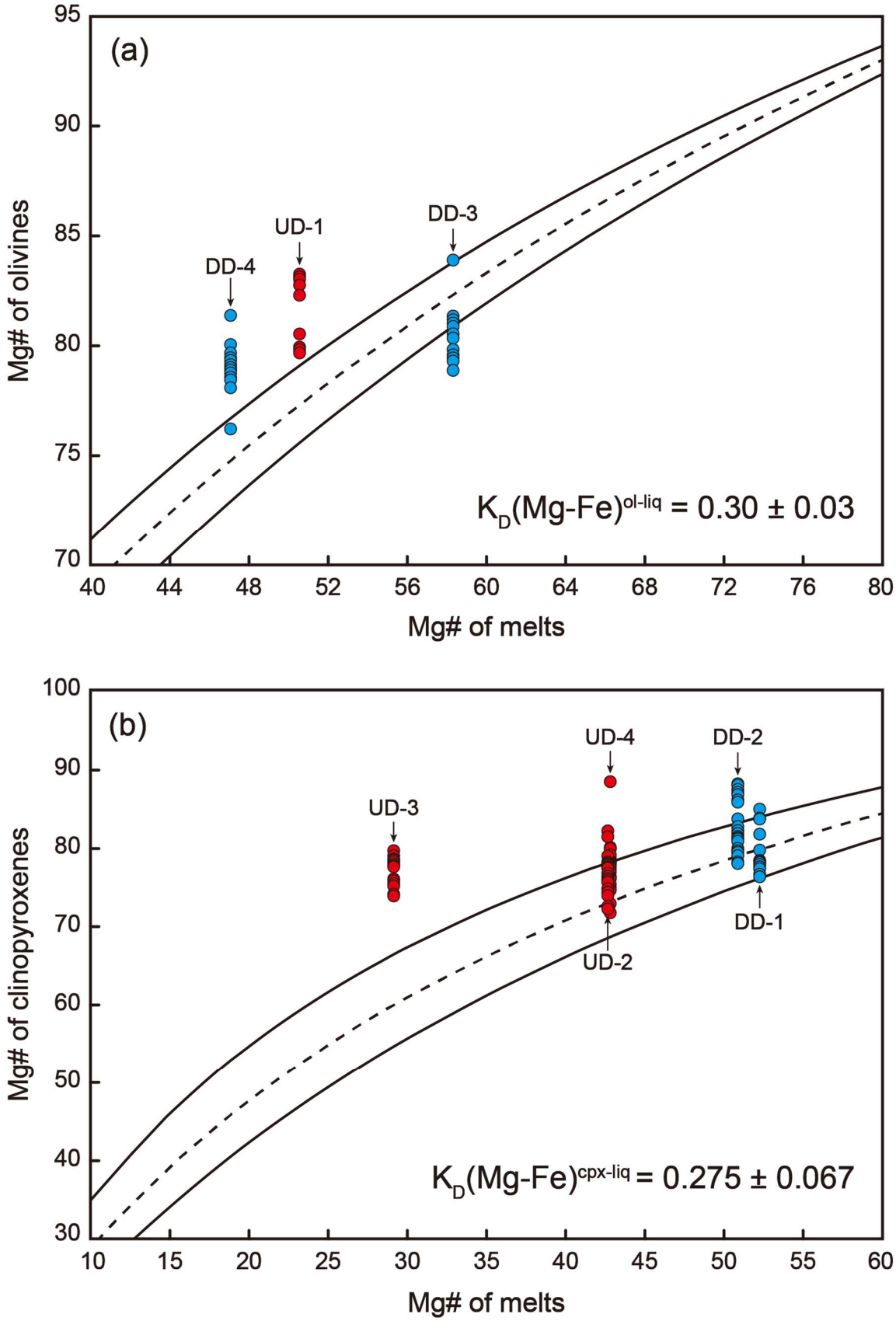
(a)
Mg# of olivines
Mg# of melts
DD-4
UD-1
DD-3
$K_D(Mg\text{-}Fe)^{ol\text{-}liq} = 0.30 \pm 0.03$
(b)
Mg# of clinopyroxenes
Mg# of melts
UD-3
UD-4
DD-2
UD-2
DD-1
$K_D(Mg\text{-}Fe)^{cpx\text{-}liq} = 0.275 \pm 0.067$

921

Fig. 6. Crystal-melt equilibrium diagrams for (a) olivine and (b) clinopyroxene included in the DU volcanic rocks. The curved solid lines indicate the range of equilibrium between minerals and melts, calculated using Fe/Mg distribution coefficients ($K_D(Mg\text{-}Fe)^{mineral\text{-}melt}$) for olivine (0.3±0.03) and clinopyroxene (0.275±0.067) (Putirka, 2008). Blue and red circles indicate values from the Dokdo and Ulleungdo basaltic samples, respectively.

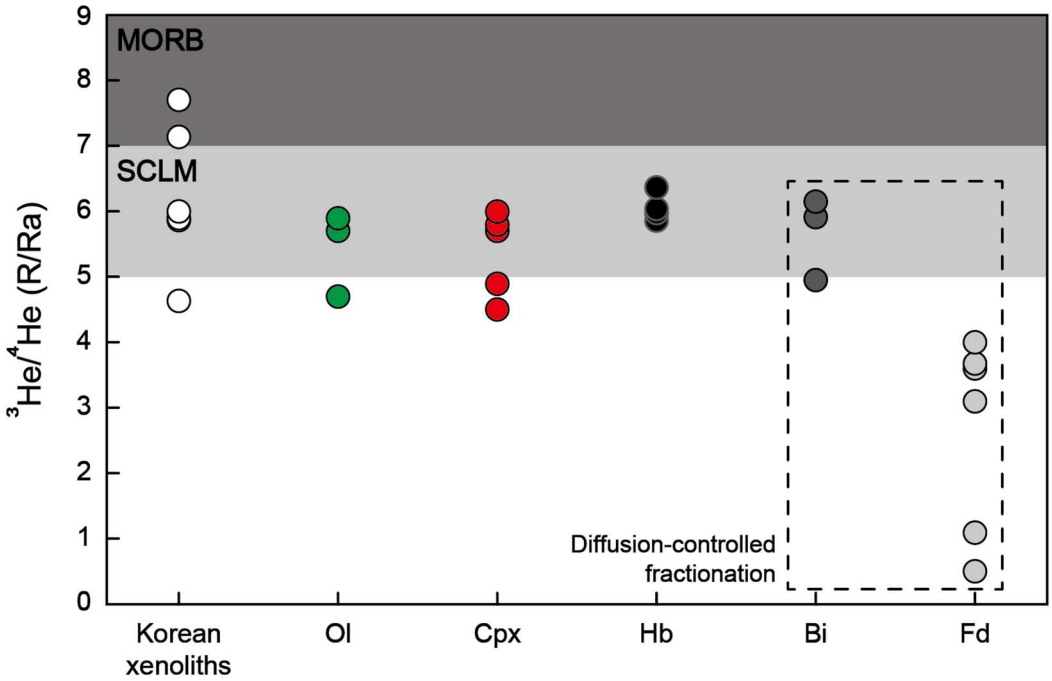

Fig. 7. Helium isotope ratios of olivine (Ol) and clinopyroxene (Cpx) from the DU basaltic rocks (this study). $^3He/^4He$ ratios of hornblende (Hb), biotite (Bt), and feldspar (Fd) are from the Ulleungdo monzonite (Kim et al., 2008). Helium isotope values from the Korean mantle xenoliths are from Kim et al. (2005). The symbols and MORB and SCLM ranges are the same to Fig. 5.

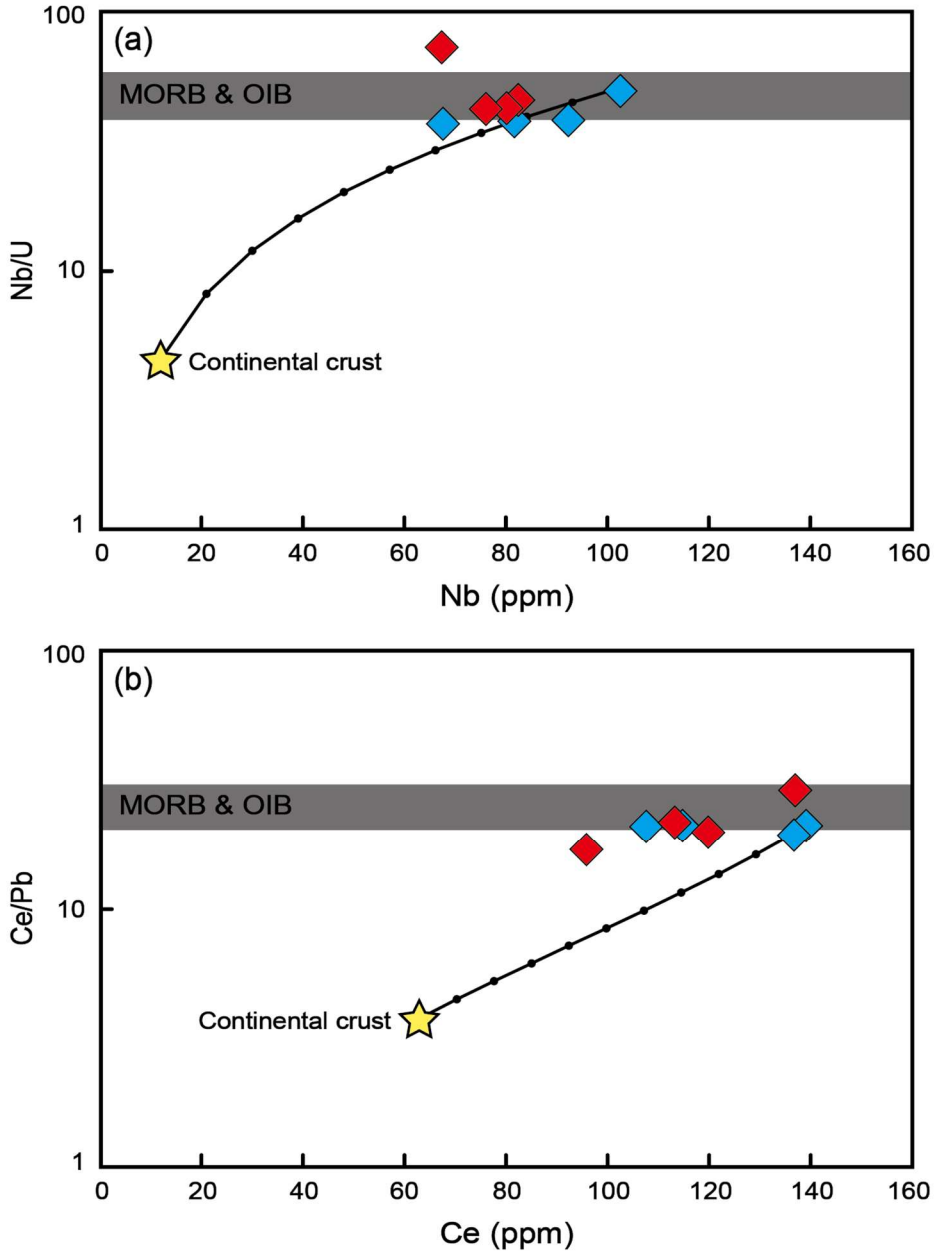

Fig. 8. (a) Nb/U versus Nb and (b) Ce/Pb versus Ce diagrams for the DU basaltic rocks to show the continental crustal effects. The average Nb/U and Ce/Pb ratios in OIB and MORB are from Hofmann et al. (1986), and the continental crust value is from Rudnick and Gao (2003). The lines with dots are simple mixing lines between DD-3 and continental crust.

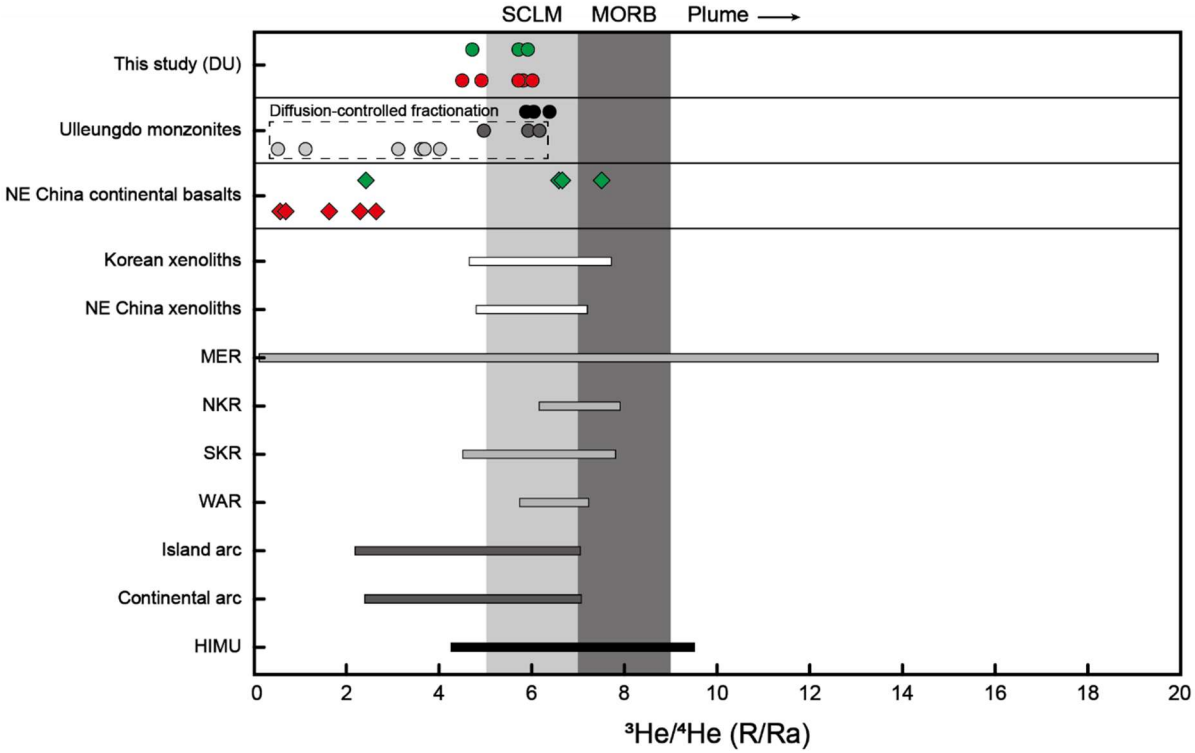

Fig. 9. Ranges of helium isotope values of the East Asian regions and various tectonic settings. References of reported $^{3}He/^{4}He$ ratios are as following [DU basaltic rocks: this study, Ulleungdo monzonites: Kim et al. (2008), NE China continental basalts: Xu et al. (2014), Korean xenoliths: Kim et al. (2005), NE China xenoliths: Chen et al. (2007), East African Rift (MER = Main Ethiopian Rift; NKR = Northern Kenya Rift; SKR = Southern Kenya Rift): Halldórsson et al. (2014) and references therein, WAR = Western Antarctic Rift: Nardini et al. (2009), island/continental arc-related volcanism: Hilton et al. (2002), HIMU mantle: Graham et al. (1992); Hanyu and Kaneoka (1997)]. The symbols and MORB and SCLM ranges are the same to Fig. 5.

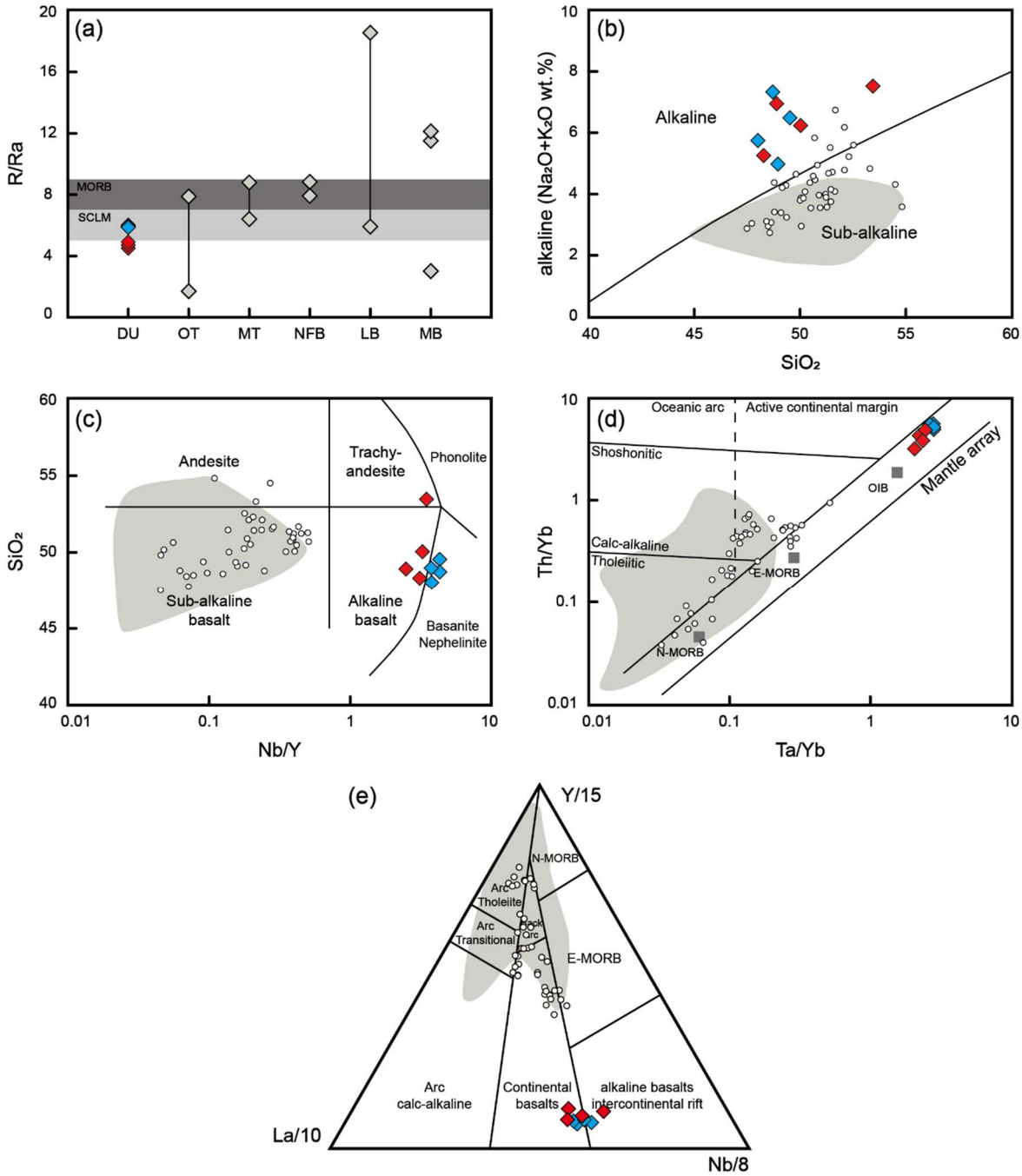

Fig. 10. (a) Helium isotope ratios of the DU basalts (this study) and several BABBs or volcanic/hydrothermal fluids. Helium isotope data of BABBs are from Okinawa Trough (Ishibashi et al., 1995; Yu et al., 2016), Mariana Trough (Ikeda et al., 1998; MacPherson et al., 2000), North Fiji basin (Nishio et al., 1998), Lau basin (Hilton et al., 1993; Lupton et al., 2015), and Manus basin (Shaw et al., 2004). (b–e) Various geochemical diagrams using major and

trace elements to distinguish the DU samples from other BABBs. Previously reported geochemical data from BABBs has references as following: Mariana Trough (Ishizuka et al., 2010), Okinawa Trough (Shinjo et al., 1999), Lau basin, and Manus basin (Jenner et al., 2012). To compare with the DU samples, the BABBs consisting of the oceanic crust of the Yamato and Japan basins in the East Sea (sites 794, 795, and 797; Allan and Gorton, 1992; Hirahara et al., 2015) are also shown as open circles.

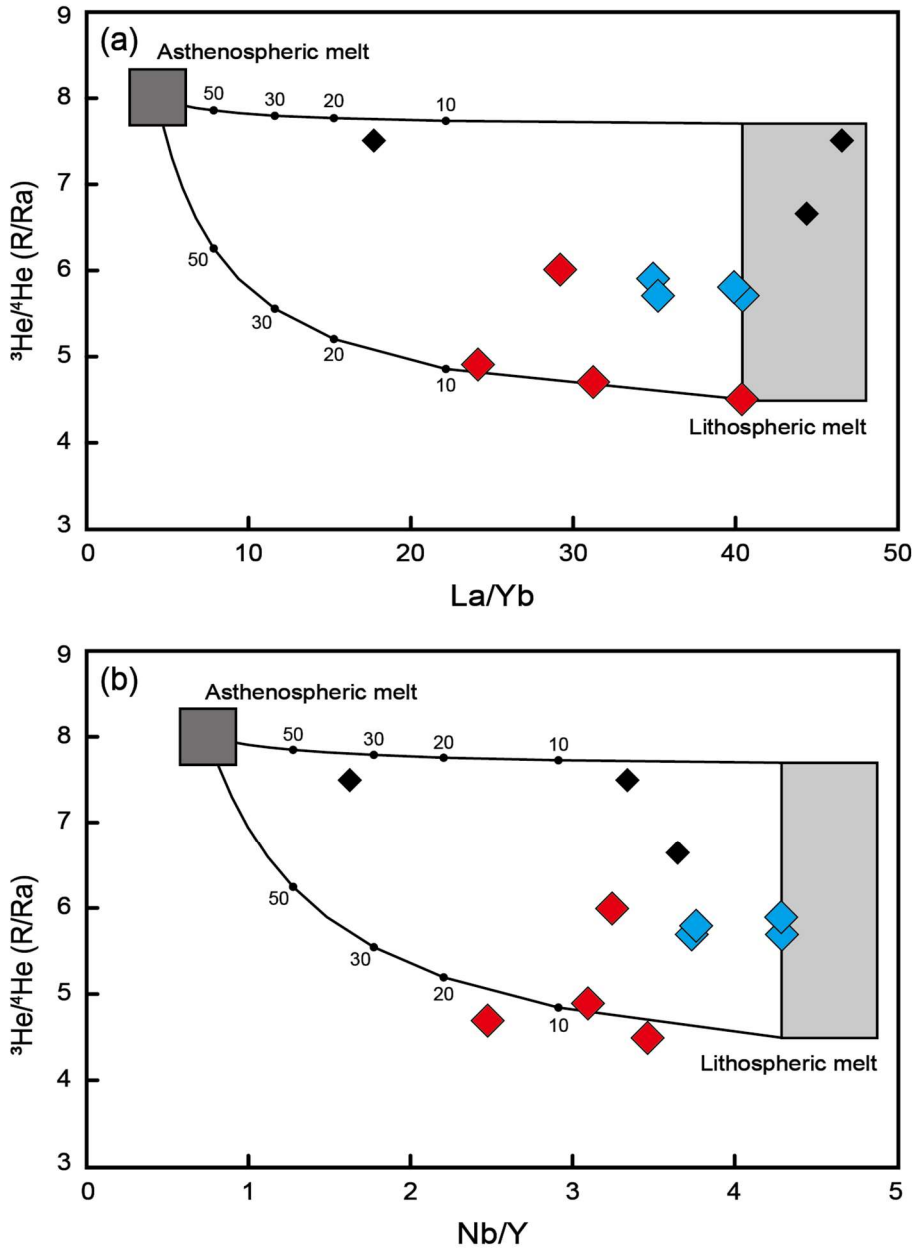

Fig. 11. Diagrams showing the results of a two-component mixing model between lithospheric and asthenospheric melts using helium isotopes and trace elements. The end-member composition of the asthenospheric melts was assumed to be the composition of popping rocks (Jones et al., 2019). The lithospheric melt end-member was assumed to have the highest ratios from the DU samples, and the helium isotope range was applied in the range (4.5 to 7.7 Ra) reported in basalts and mantle xenoliths in East Asia (this study; Chen et al., 2007; Kim et al., 2005). The solid lines represent the two-component mixing relationships with the mixing ratios

(asthenospheric melt percentage contribution). For reference, the Cenozoic basalt of Changle-Linqu (NE China) located in eastern NCC is indicated by black diamonds (Chen et al., 2007).

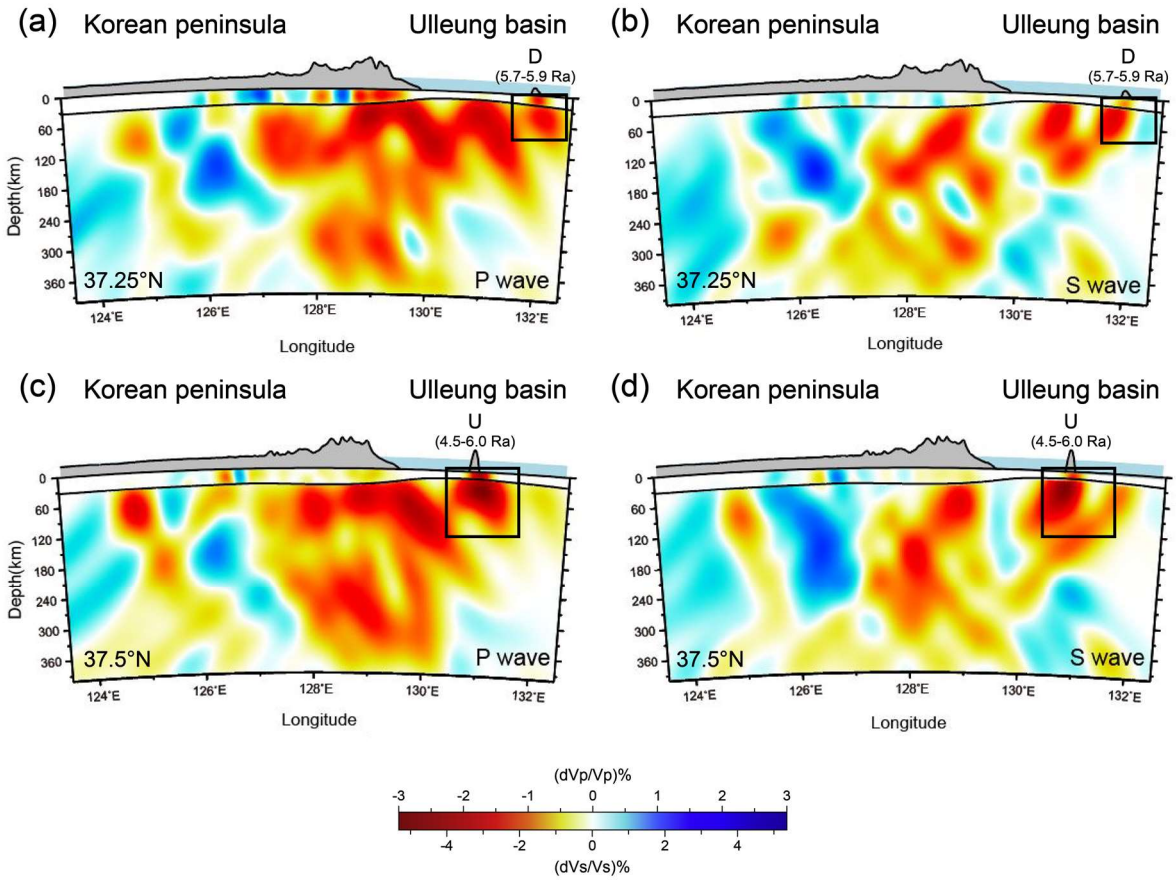

Fig. 12. (a–d) Vertical cross-sections of seismic *P*- and *S*-wave tomography for Dokdo at latitude 37.25°N (a, b) and Ulleungdo at latitude 37.5°N (c, d) (Song et al., 2020). Moho depths are displayed as solid lines beneath the surface. Resolution of tomographic models is provided in Fig. S6. Low-velocity zones beneath the DU volcanoes (black squares) indicate the lithosphere-asthenosphere interaction.